PhD Thesis

PRMT1-mediated methylation of MICU1 is a key for the engagement of UCP2 in mitochondrial Ca^{2+} uptake

submitted by

Mag.pharm. Corina

MADREITER-SOKOLOWSKI

attaining the academic degree

Doctor of Philosophy (PhD)

at the

Medical University of Graz

conducted at the

Institute of Molecular Biology and Biochemistry

under the supervision of

Univ.-Prof. Dr.rer.nat. Wolfgang F. Graier

2016

DECLARATION

Affidavit

I, hereby, declare that the following thesis has been written only by myself and that I have fully acknowledged by name all of those individuals and organisations that have contributed to the research for this thesis. Furthermore, I confirm that no sources have been used in the preparation of this thesis other than those indicated in the thesis itself. Throughout this thesis and in all related publications I followed the guidelines of "Good Scientific Practice".

Graz, …… *Signature*

Eidesstattliche Erklärung

Ich erkläre ehrenwörtlich, dass ich die vorliegende Arbeit selbständig verfasst habe und jene Personen, die am Zustandekommen der Forschungsdaten beteiligt waren, namentlich genannt habe. Andere als die angegebenen Quellen habe ich nicht verwendet und die den benutzten Quellen wörtlich oder inhaltlich entnommenen Stellen habe ich als solche kenntlich gemacht. Die Arbeit an der Dissertation und daraus entstandener Publikationen wurde gemäß den Regeln der „Good Scientific Practice" durchgeführt.

Graz, am …… *Unterschrift*

ACKNOWLEDGEMENT

Am Ende meines Studiums gebührt mein Dank jenen, die mich all die Studienjahre hindurch unterstützt und auf diese Weise maßgeblich zum Gelingen dieser Arbeit beigetragen haben.

Mein besonderer Dank gilt meinem Supervisor **Univ.-Prof. Dr.rer.nat. Wolfgang Graier**, der mein Tun mit viel Geduld und konstruktiver Kritik in die richtige Richtung gelenkt hat und mir mit seiner unerschütterlichen Leidenschaft für die Wissenschaft immerzu mit Rat und Tat zur Seite stand.

Ein spezieller Dank gilt all meinen Kolleginnen und Kollegen, die maßgeblich zum Gelingen und auch zur Freude an meiner Arbeit beitragen haben. Hervorheben möchte ich **Christiane Klec, MSc.** und **Mag.pharm. Warisara Parichatikanond, PhD**, die einen weiten Weg mit mir gemeinsam bestritten haben und in dieser Zeit zu lieben Freundinnen geworden sind. Weiters möchte ich mich bei Frau **Dr.rer.nat. Sonja Barth** ganz herzlich für ihre guten Ratschläge und Ideen bedanken, die mir in den letzten Jahren und beim Erstellen dieser Arbeit sehr hilfreich waren.

Meinen Eltern **Rosemarie Nitzinger** und **Wolfgang Madreiter** sowie meinen Großeltern danke ich von ganzem Herzen für den jahrelangen Rückhalt und dafür, dass sie meine Interessen immerzu gefördert und unterstützt haben. Hervorheben möchte ich auch meine liebe Godi **Theresia Nitzinger**, die mich in schwierigen Zeiten oft aufgemuntert hat. Danken möchte ich auch meiner lieben Schwester **Lisa Marie Madreiter**, die sich in den letzten Jahren als geduldige Zuhörerin erwiesen hat und unseren gemeinsamen Traum von einer Musikkarriere verwirklicht. Darüber hinaus gilt auch meinen Schwiegereltern **Malgorzata Sokolowski** und **Dr.med. Adam Sokolowski**, die während meines Studiums eine große Stütze waren, mein Dank.

Zu guter Letzt möchte ich meinem lieben Partner **Dr.med.univ. Dr.med.dent. Armin Sokolowski** dafür danken, dass er mich in meiner gesamten Studienzeit aufopfernd unterstützt hat und immerzu bestmöglich zur Verwirklichung meiner Ideen und Pläne beiträgt.

ABSTRACT

Mitochondria are supplying the cell with adenosine triphosphate (ATP) and are essential for cell differentiation, cell cycle, and intracellular signaling. The transfer of the ubiquitous second messenger Ca^{2+} into the matrix of mitochondria is an important process that substantially contributes to these cellular functions. Recent studies demonstrated that mitochondrial Ca^{2+} uptake is achieved by a macromolecular complex, which basically consists of the pore-forming mitochondrial Ca^{2+} uniporter (MCU) protein, the essential MCU regulator (EMRE) and the mitochondrial Ca^{2+} uptake 1 (MICU1). MICU1 is a Ca^{2+} sensing protein, which interacts with MCU in order to prevent mitochondrial Ca^{2+} overload potentially leading to cell stress and death. Before characterization of these proteins, uncoupling proteins 2 and 3 (UCP2/3) have been demonstrated to be crucial for mitochondrial Ca^{2+} uptake. Nevertheless, the mechanism how UCP2/3 contribute to mitochondrial Ca^{2+} uptake remained controversial. To clarify this issue we screened different cell types regarding the role of UCP2/3 in mitochondrial Ca^{2+} uptake by using genetically encoded fluorescent Ca^{2+} probes as well as fluorescent dyes. While modulation of UCP2/3 expression strongly affected mitochondrial Ca^{2+} uptake in HeLa and Ea.hy926, an UCP2/3-insensitive mitochondrial Ca^{2+} uptake could be identified in human umbilical vein endothelial cells (HUVECs) as well as in porcine aortic endothelial cells (PAECs). Western blots revealed a strongly increased asymmetric arginine dimethylation state of UCP2/3-dependent HeLa and Ea.hy926 in comparison to UCP2/3-independent HUVECs and PAECs. Förster resonance energy transfer (FRET)-based mitochondrial Ca^{2+} measurements and proteomic analyses demonstrated that protein arginine methyl transferase 1 (PRMT1) modulates mitochondrial Ca^{2+} uptake by asymmetrical methylation of MICU1. Methylation of MICU1 resulted in a decrease of its Ca^{2} sensitivity leading to attenuated mitochondrial Ca^{2+} uptake. It could be shown, that UCP2/3 normalized Ca^{2+} sensitivity of MICU1 and, thus, restored mitochondrial Ca^{2+} uptake in case of elevated PRMT1 activity. Since PRMT1 activity was reported to be highly elevated in certain types of cancer, these data not just provide novel insights in the complex regulation of the mitochondrial Ca^{2+} uptake, but also unveil possible targets for cancer treatments in the future.

ZUSAMMENFASSUNG

Mitochondrien versorgen die Zelle mit Adenosintriphosphat (ATP) und sind maßgeblich an Zelldifferenzierung, Regulation des Zellzyklus sowie an der intrazellulären Signalweitergabe beteiligt. Die Aufnahme des sekundären Botenstoffes Ca^{2+} in die mitochondrielle Matrix trägt entscheidend zu den genannten Prozessen bei. Kürzlich veröffentlichte Arbeiten zeigten, dass ein makromolekularer Komplex die mitochondrielle Ca^{2+} Aufnahme sicherstellt. Wesentliche Bestandteile dieses Komplexes sind der Poren bildende mitochondrielle Ca^{2+} Uniporter (MCU), der essentielle MCU Regulator (EMRE) und der mitochondrielle Ca^{2+} Uptake 1 (MICU1). Das Protein MICU1 agiert als Ca^{2+} Sensor, welcher mit MCU interagiert, um eine übersteigerte mitochondrielle Ca^{2+} Aufnahme, die zu zellulärem Stress und letztlich zum Zelltod führen kann, zu verhindern. Vor der Charakterisierung genannter Proteine, konnte bereits gezeigt werden, dass die Uncoupling Proteine 2 und 3 (UCP2/3) entscheidend in der mitochondriellen Ca^{2+} Aufnahme sind. Allerdings blieb umstritten, wie UCP2/3 an der mitochondriellen Ca^{2+} Aufnahmen beteiligt sind. Um dies zu klären, wurden verschiedene Zelltypen hinsichtlich der Rolle von UCP2/3 in der mitochondriellen Ca^{2+} Aufnahme mithilfe von genetisch kodierten, fluoreszierenden Ca^{2+} Sensoren sowie Farbstoffen untersucht. Während die Modulation der UCP2/3 Expression einen starken Effekt auf die mitochondrielle Ca^{2+} Aufnahme in HeLa und Ea.hy926 Zellen zeigte, wurde eine UCP2/3-unabhängige mitochondrielle Ca^{2+} Aufnahme in humanen Nabelschnurendothelzellen (HUVECs) sowie in Endothelzellen von Schweineaorten (PAECs) gefunden. Mithilfe von Western Blots wurden, im Vergleich zu den UCP2/3-unabhängigen HUVECs und PAECs, stark erhöhte Spiegel an asymmetrischen Arginin Dimethylierungen in den UCP2/3-abhängigen HeLa und Ea.hy926 Zellen nachgewiesen. Weiters zeigten Förster-Resonanzenergietransfer (FRET)-basierte mitochondrielle Ca^{2+} Messungen sowie proteomische Analysen, dass die Protein Arginine Methyltransferase 1 (PRMT1) den mitochondrielle Ca^{2+} Aufnahme über die asymmetrische Methylierungen von MICU1 kontrolliert. Methylierung von MICU1 führt zu verringerter Ca^{2+} Sensitivität und daraus folgend zu einer schwächeren mitochondriellen Ca^{2+} Aufnahme. Bei erhöhter PRMT1 Aktivität normalisierten UCP2/3 aber die Ca^{2+} Sensitvität von MICU1 und sicherten auf diese Weise die mitochondrielle Ca^{2+} Aufnahme. Da in verschiedenen Krebsarten eine erhöhte PRMT1 Aktivität vorliegt, zeigen diese Daten nicht nur eine neuartige Regulation der mitochondriellen Ca^{2+} Aufnahme auf, sondern enthüllen auch Angriffspunkte für Krebstherapien der Zukunft.

LIST OF ABBREVIATION

Acetyl-CoA	Acetyl coenzyme A
ADMA	Asymmetric dimethylarginine
AdOx	Adenosine-2′,3′-dialdehyde
ADP	Adenosine diphosphate
ATP	Adenosine triphosphate
BAD	Bcl-2 antagonist of cell death
Bcl-2	B-cell lymphoma 2
BMCP1	Brain mitochondrial carrier protein-1
BMCP1	Brain mitochondrial carrier protein-1
BSA	Bovine serum albumin
CaM	Calmodulin
CFP	Cyan fluorescent protein
D-cpv	Circularly permuted Venus
DMEM	Dulbecco's modified eagle medium
DNA	Desoxyribonucleic acid
Drp1	Dynamin-related protein 1
EGM-2	Endothelial cell growth medium-2
EMRE	Essential MCU regulator
ER	Endoplasmic reticulum
ETC	Electron transport chain
$FADH_2$	Flavine adenine dinucleotide
FBS	Fetal bovine serum
FP	Fluorescent protein
FRET	Förster resonance energy transfer
Fura-2/AM	Fura-2/acetoxymethyl ester
GAPDH	Glyceraldehyde 3-phosphate dehydrogenase
GECI	Genetically encoded calcium indicators
Grp75	Glucose-regulated protein 75
HUVEC	Human umbilical vein endothelial cell
IML2	Intermembrane loop 2

IMM	Inner mitochondrial membrane
IMS	Intermembrane space
IP	Immunoprecipitation
IP3R	Inositol trisphosphate receptor
ITC	Isothermal titration calorimetry
K_d	Dissociation constant
Letm1	Leucine zipper-EF-hand containing transmembrane protein 1
MAM	Mitochondrial ER-associated membrane
mCa1	mitochondrial Ca^{2+} current type 1
mCa2	mitochondrial Ca^{2+} current type 2
MCU	Mitochondrial calcium uniporter
MCUb	Mitochondrial calcium uniporter b
MCUR1	Mitochondrial calcium uniporter regulator 1
Mfn1	Mitofusin 1
Mfn2	Mitofusin 2
MICU1	Mitochondrial calcium uptake 1
MICU2	Mitochondrial calcium uptake 2
MMA	Monomethylarginine
mRyR1	Mitochondrial ryanodine receptor 1
MS	Mass spectrometry
mtDNA	Mitochondrial DNA
NADH	Nicotinamide adenine dinucleotide
NCLX	Mitochondrial $Na^{+/}Ca^{2+}$ exchanger
NCX	Na^{+}/Ca^{2+} exchanger
NMDAR	N-methyl-D-aspartate receptor
OMM	Outer mitochondrial membrane
OPA1	Optic atrophy 1
OXPHOS	Oxidative phosphorylation
PAEC	Porcine aortic endothelial cell
PBS	Phosphate-buffered saline
PMCA	Plasma membrane Ca^{2+} ATPase
PRMT	Protein arginine methyltransferase

pS	Picosiemens
PTM	Post translational modification
PTP	Permeability transition pore
qRT-PCR	Quantitative real-time polymerase chain reaction
RaM	Rapid mode of Ca^{2+} uptake
RIPA	Radioimmunoprecipitation assay
RNA	Ribonucleic acid
ROS	Reactive oxygen species
SDMA	Symmetric dimethylarginine
SERCA	Sarco/endoplasmic reticulum Ca^{2+} ATPase
siRNA	Small interfering ribonucleic acid
SOCE	Store-operated Ca^{2+} entry
STIM1	Stromal interaction molecule-1
TCA	Tricarboxylic acid
TCGA	The cancer genom atlas
TMD	Transmembrane domain
TRPC3	Transient receptor potential cation channel 3
UCP2	Uncoupling protein 2
UCP3	Uncoupling protein 3
VDAC	Voltage-dependent anion channel
xIMCC	Extra-large mitochondrial Ca^{2+} current
YFP	Yellow fluorescent protein

TABLE OF CONTENTS

1 INTRODUCTION

1.1 Mitochondria's origin and structure

Mitochondria (Figure 1.1) are ancient, worm-like and dynamic compartments of eukaryotic cells, which occurred about two billion years ago most likely by incorporation of an α-proteobacterium into an ancestor of the modern eukaryotic cell (1). While mitochondria's double-membrane as well as the ability for adenosine triphosphate (ATP) production were preserved, the structure developed and additional functions were gained. Although the majority of the α-proteobacterial genomic material got lost, a circular genome in the size of approximately 16 kilobases remained, including genetical information for 13 proteins of the mitochondrial respiratory complexes (2). Since mammalian mitochondria consist of more than 1500 proteins, except from 13 proteins encoded by the nuclear genome and synthesized in the cytosol, these organelles strongly rely on actively imported mitochondrial proteins derived from nucleus and other cellular compartments (3). Due to their supposed origin mitochondria are enclosed by two functionally distinct membranes composed of phospholipid bilayers and proteins. The outer mitochondrial membrane (OMM), barrier between cytosol and intermembrane space (IMS), exhibits a large number of pores, such as the voltage-dependent anion channel VDAC (4). These pores allow a concentration gradient driven diffusion of molecules such as adenine nucleotides or cations up to approximately 6 kDa (5). If this size is exceeded, proteins can be actively transported through the membrane by high-molecular-weight complexes, so called translocases, which recognize specific signaling sequences at the proteins' N-terminus (6). The OMM also ensures the interplay between mitochondria and the cellular environment. While the OMM is the barrier between cytosol and IMS, the inner mitochondrial membrane (IMM) separates the IMS from the mitochondrial matrix, exhibiting an extraordinary high protein to phospholipid ratio due to essential processes happening there. Since the IMM is impermeable to all molecules, specific transport systems and channel-forming proteins are necessary for the molecules' entry into the mitochondrial matrix (7, 8). The mitochondrial respiration chain, the most essential function of mitochondria, is embedded in

the IMM. Numerous infoldings, stretching deeply into the mitochondrial matrix, greatly increase the surface area of the IMM and, therefore, enhance the mitochondria's ATP production, the essential energy „currency" of the cell. The mitochondrial matrix is crucial for ATP production, because of its high pH, which is a driving force for the electrochemical gradient. Besides, it houses numerous enzymes as well as mitochondrial desoxyribonucleic acid (DNA) and is the site of the citric acid cycle (4).

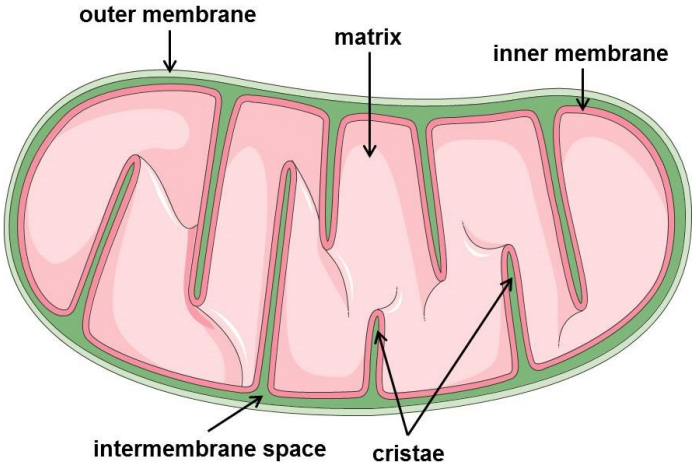

Figure 1.1: Scheme of mitochondrial structure. [adopted from *Servier medical art*]

Mitochondria change their morphological appearance rapidly according to their environment and their demand (Figure 1.2). Different GTPases are responsible for mitochondrial fusion, including mitofusin 1 (Mfn1) and mitofusin 2 (Mfn2) in the OMM as well as optic atrophy 1 (OPA1) in the IMM, and fission, as, for instance, dynamin-related protein 1 (Drp1) (9). With the help of these proteins, mitochondria continuously undergo fission and fusion to ensure cell survival and adaptation to occurring conditions as, for instance, cell growth, division or differentiation.

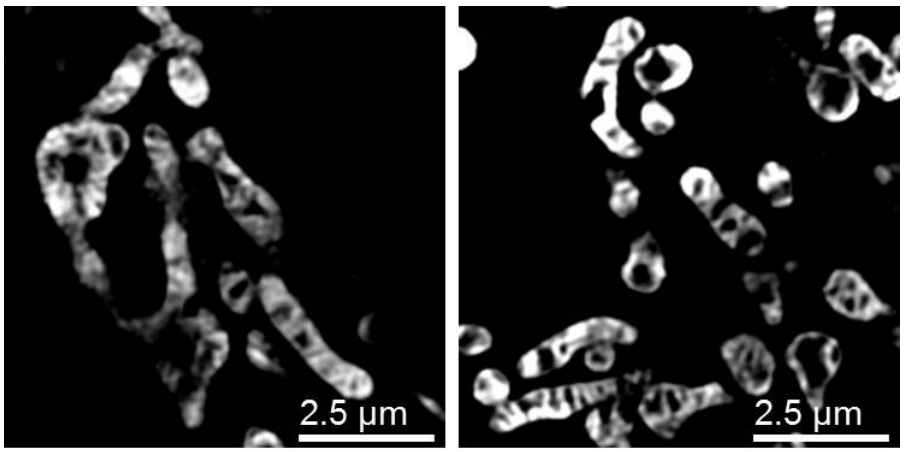

Figure 1.2: Fusion and fission of mitochondria. Images showing intact mitochondria *(left panel)* and mitochondria after histamine-induced fission *(right panel)*. Mitochondria were stained with MitoTrackerRed® CMXRos and recorded on a Nikon-structured illumination microscope by my colleague Benjamin Gottschalk.

1.2 Mitochondrial function

The central tasks of mitochondria are ATP production through oxidative phosphorylation (OXPHOS) (Figure 1.3) and control of cellular metabolism (10, 11). In addition to energy supply, mitochondria play a key role in the calcium sequestration (12, 13) and numerous physiological processes including cell differentiation (14-16), cell cycle control (17, 18), and intracellular signaling (19). Therefore, they are also involved in various pathological conditions, such as cancer (20, 21), cardiovascular dysfunction (22, 23), and neurodegenerative diseases (24-26).

1.2.1 Energy supply

An average adult human requires approximately 420 kJ per hour at resting condition, which corresponds with the production of roughly 65 kg of ATP per day, representing a Herculean task to mitochondria (27). Mitochondria have a main role in the energy metabolism (Figure 1.3). While carbohydrate cleavage via glycolysis, taking place in the cytosol, yields just small amounts of ATP, oxidation of glycolysis derived pyruvate and nicotinamide adenine dinucleotide (NADH) by mitochondria generates about 15 times more ATP (28). Acetyl coenzyme A (Acetyl-CoA), derived from oxidative decarboxylation of pyruvate or beta-oxidation in the mitochondrial matrix, fuels the tricarboxylic acid (TCA) cycle to produce NADH and flavin adenine dinucleotide ($FADH_2$), which are then used as electron donors for the electron transport chain (ETC). The mechanism of ATP generation by mitochondria remained elusive until Peter D. Mitchell presented his groundbreaking chemiosmotic theory in 1961.

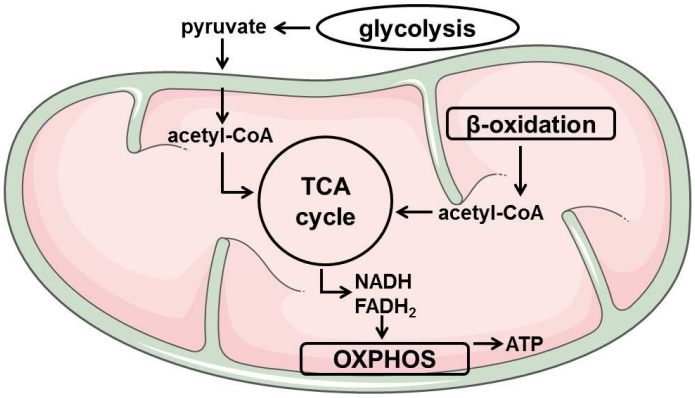

Figure 1.3: Scheme of mitochondrial metabolism. [adopted from *Servier medical art*]

The machinery of OXPHOS is built up by the ETC, consisting of NADH dehydrogenase (complex I), succinate dehydrogenase (complex II), ubiquinone, cytochrome bc1 complex (complex III), as well as cytochrome c and cytochrome c oxidase (complex IV). After transfer of electrons, derived from the NADH and $FADH_2$ as hydrogen molecules, to the ETC via complex I and II, the electron transport through complex I to complex IV is coupled to proton pumping from the mitochondrial matrix into the IMS. This process causes a negative charge in the matrix and a positive charge in the IMS resulting in an electrochemical gradient, used for the proton transport back from the IMS into the mitochondrial matrix through ATP synthase (complex V). The released energy is, finally, utilized by ATP synthase to gain the cellular current, ATP, by phosphorylation of adenosine diphosphate (ADP) (11).

1.2.2 Calcium sequestration

Mitochondrial Ca^{2+} buffering is either linked to the capacitive Ca^{2+} influx through the plasma membrane (29) or to the Ca^{2+} release from the main internal Ca^{2+} store, the endoplasmic reticulum (ER) (30). While voltage-gated Ca^{2+} channels in the plasma membrane are predominantly involved in cellular Ca^{2+} influx in excitable cells, Ca^{2+} entry in non-excitable cells occurs mostly through ligand-gated, receptor-operated, second messenger-operated, store-operated or stretch-operated channels (31). In order to regulate cytosolic Ca^{2+} level after Ca^{2+} entry and to control Ca^{2+} homeostasis, the Na^{+}/Ca^{2+} exchanger (NCX) as well as plasma membrane Ca^{2+} ATPase (PMCA) ensure the extrusion of Ca^{2+} from the cell (32) and an intensive interplay between plasma membrane and ER as well as plasma membrane and mitochondria takes place. The close contact between plasma membrane and ER can be demonstrated by a process known as store-operated Ca^{2+} entry (SOCE). In this process low Ca^{2+} levels in the ER cause oligomerization and, finally, a conformational change of the Ca^{2+} sensing stromal interaction molecule-1 (STIM1), which then activates the plasma membrane Ca^{2+} channel ORAI1 by protein-protein interaction causing Ca^{2+} entry (33). The Ca^{2+} interplay between mitochondria and ER occurs mainly in regions of mitochondrial ER-associated membranes (MAMs), where ER tubules are closely tethered to mitochondria (34, 35) by linking proteins like glucose-regulated protein 75 (grp75) (36) and mitofusin 2 (37) in order to allow lipid transfer and to create a Ca^{2+} hub.

Within these regions, a sophisticated toolkit ensures transport and control of Ca^{2+} ions (Figure 1.4). The sarco/endoplasmic reticulum Ca^{2+} ATPase (SERCA) transfers Ca^{2+} from the cytosol into the lumen of the ER, from where Ca^{2+} is released by activation of inositol trisphosphate receptor (IP3R) (38). Once released into the cytosol, Ca^{2+} has to be rapidly removed again in order to restore resting conditions. This is partly achieved by SERCA pumping back Ca^{2+} into the ER, but mainly by mitochondria taking up Ca^{2+} rapidly through the VDAC in the OMM and a mitochondrial Ca^{2+} uptake complex in the IMM. In mitochondria accumulated Ca^{2+} is released into the cytosol through the mitochondrial Na^{+}/Ca^{2+} exchanger (NCLX) (39). The transfer of the ubiquitous second messenger Ca^{2+} into the mitochondrial matrix is an important signaling process that substantially contributes to physiological and pathophysiological pathways (Figure 1.4).

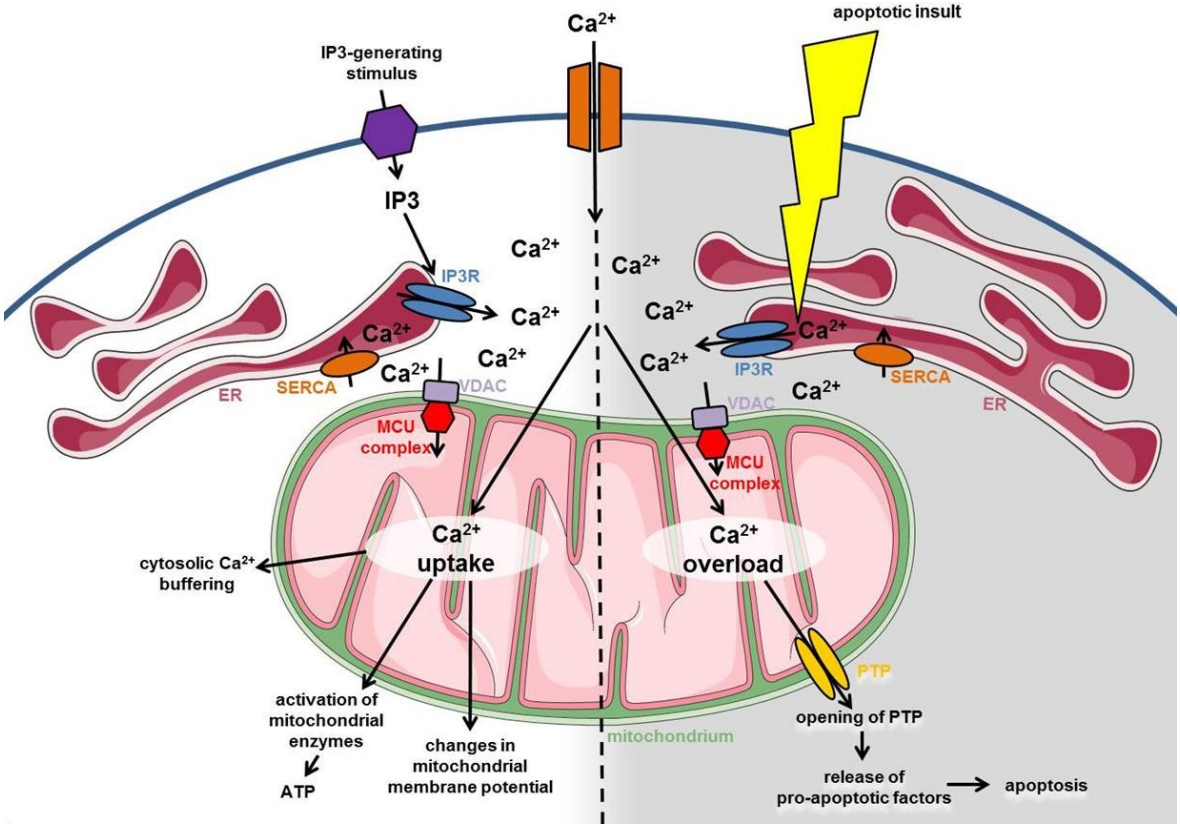

Figure 1.4: Life and death pathways triggered by mitochondrial Ca^{2+} accumulation.
[modified and adopted from Hung et. al., 2010, (40)]

For instance, metabolic activity is strongly influenced by Ca^{2+}-dependent mitochondrial enzymes of the TCA cycle like pyruvate dehydrogenase (41), isocitrate dehydrogenase (42), and alpha-ketoglutarate dehydrogenase (43). Furthermore, mitochondrial Ca^{2+} import, which is not accompanied by any other ion exchange, causes changes in mitochondrial membrane potential (44).

Mitochondria also buffer cytosolic calcium overload and therefore regulate Ca^{2+} concentration in cellular microdomains. Among other things, this causes alterations in the activity of cytosolic Ca^{2+}-dependent enzymes like calcium-calmodulin dependent protein kinases (45). On the other hand mitochondrial Ca^{2+} accumulation can have a harmful effect, as it may lead to the opening of mitochondrial permeability transition pore (PTP) (46), which causes the release of mitochondrial apoptotic factors into the cytosol and, finally, apoptosis (47).

1.3 Mitochondrial Ca^{2+} uptake machinery

1.3.1 A historical overview

Despite its importance the nature of mitochondrial Ca^{2+} homeostasis remained a mystery over more than 50 years and was subject of intensive research (Figure 1.5). Experiments in the 1950s had already unveiled Ca^{2+}-induced mitochondrial swelling, which was related to non-osmotic reasons (48, 49). The mere ability of isolated mitochondria to take up Ca^{2+} from the medium and to accumulate it in the mitochondrial matrix in an energy-driven process was, finally, unveiled 1961 by an indirect measurement of extra-mitochondrial Ca^{2+} level reduction (50). Moreover, in parallel to the acceptance of the chemiosmotic hypothesis, the membrane potential of the inner mitochondrial membrane was found to be the main driving force for Ca^{2+} accumulation (11). The discovery of a specific inhibitor of the mitochondrial Ca^{2+} uptake process, ruthenium red, additionally facilitated the search for a hypothetical uniporter (51, 52). Nevertheless, it was a long matter of debate, if one or two positive charges are transported across the membrane by either a H^+/Ca^{2+} antiporter (53) or by a Ca^{2+}-carrying mitochondrial Ca^{2+} uniporter, MCU (54), respectively. After the scientific community agreed on an MCU-mediated mitochondrial Ca^{2+} uptake, the striking finding that the affinity of MCU for Ca^{2+} was in a non-physiological, very low range with a KD value of 20-30 µM came up (55). Therefore, MCU-mediated Ca^{2+} uptake was dismissed as non-physiological and mitochondria were believed to be just passive Ca^{2+} sinks (56). Finally, at the beginning of the 1990s new insights regarding mitochondrial Ca^{2+} uptake were gained by the usage of genetically

encoded chemiluminescent and later fluorescent indicators targeted to mitochondria, which allowed life cell imaging. Studies with the Ca^{2+} probe aequorin revealed an enormous increase in mitochondrial matrix Ca^{2+} levels, exceeding the Ca^{2+} level of cytoplasm up to two orders of magnitude, as well as an active contribution of mitochondria in the cell's Ca^{2+} homeostasis (57, 58). The unexpected highly efficient mitochondrial Ca^{2+} uptake was explained by cytosolic microdomains with high levels of Ca^{2+}, occurring in the area between ER and mitochondria during stimulation (59). These high level Ca^{2+} regions were also expected to dissipate rapidly in order to prevent mitochondrial Ca^{2+} overload and the initiation of the apoptotic process via opening PTP (60). Although the nature of mitochondrial Ca^{2+} uptake was intensively studied over centuries, the components of the uptake machinery remained elusive. MCU was demonstrated to be an inward rectifying, highly selective Ca^{2+} ion channel not earlier than 2004 by patch-clamp data (61). In 2007, uncoupling proteins 2 (UCP2) and 3 (UCP3) were identified as essential components of the MCU-mediated Ca^{2+} uptake by Trenker et. al. (62). Two years later, leucine zipper-EF-hand containing transmembrane protein 1 (Letm1) was demonstrated to function as H^{+}/Ca^{2+} antiporter and was suggested to enable mitochondrial Ca^{2+} uptake at low cytosolic levels, while MCU is the key player in the case of higher Ca^{2+} levels (63, 64). In 2010, Vamsi Mootha and his group achieved a fundamental step forward by identifying the 54 kDa mitochondrial Ca^{2+} uptake 1 (MICU1), containing two EF-hand Ca^{2+} binding domains, as an essential regulator of MCU (65). Then, finally, the 35 kDa coiled-coil domain-containing protein CCDC109A could be identified as MCU by two different groups in parallel and was shown to possess two transmembrane domains, possibly forming a channel via oligomerization (66, 67). In 2012, mitochondrial calcium uniporter regulator 1 (MCUR1) was demonstrated to bind to MCU and to regulate ruthenium-red-sensitive MCU-dependent mitochondrial Ca^{2+} uptake (68). A dominant negative form of MCU, mitochondrial calcium uniporter b (MCUb), was characerized in 2013. This protein, which reduces the agonist stimulated mitochondrial Ca^{2+} increase, was demonstrated to have 50% sequence similarity with MCU as well as two predicted transmembrane domains (69). In 2013, a paralog of MICU1, mitochondrial calcium uptake 2 (MICU2), was observed to be a component of the MCU-MICU1 complex, showing an additive impairment in calcium handling with MICU1 (70). In this year, also the essential MCU regulator

(EMRE), a 10 kDa protein with a single transmembrane domain, was shown to be required for the interaction of MCU with MICU1 and MICU2 (71). In 2014, SLC25A23 was characterized as EF-hand domain containing mitochondrial protein, which possibly regulates mitochondrial Ca^{2+} uptake (72). It is still elusive, how all of these recently identified proteins interact with each other, but it could be demonstrated that Ca^{2+} is taken up by mitochondria via different Ca^{2+} uptake routes. It has been shown, for instance, that modification of cytosolic Ca^{2+} levels by inhibition of SERCA switches mitochondrial Ca^{2+} uptake from a UCP2/3- and MCU-dependent to a Letm1- and MCU-dependent uptake (73).

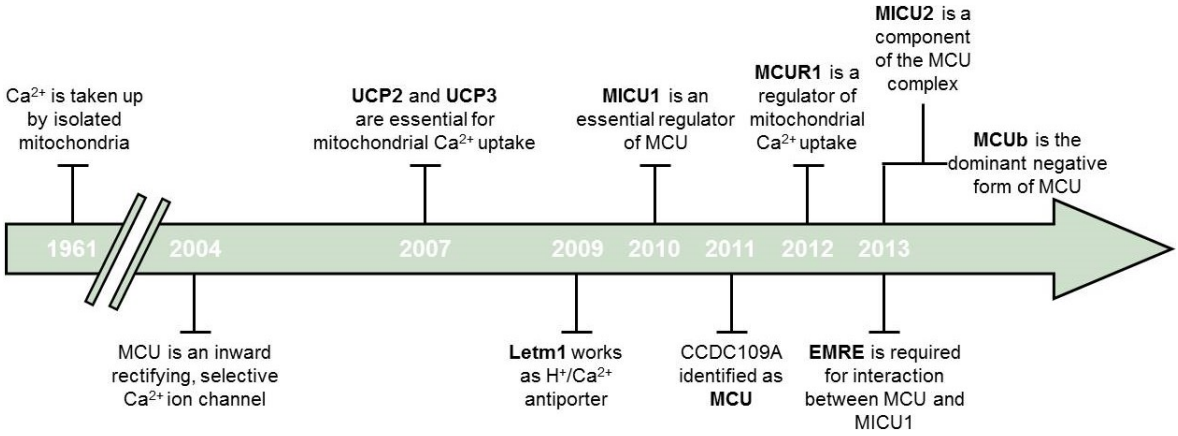

Figure 1.5: Timeline depicting the investigation process of mitochondrial Ca^{2+} uptake.

1.3.2 UCP2/3: fine-tuners of mitochondrial Ca^{2+} uptake

Uncoupling proteins are members of the large family of mitochondrial ion transporters. They function as anion carriers across the IMM by promoting H^+ flux into the mitochondrial matrix. Via that mechanism UCP1, also known as thermogenin, functions as uncoupler in brown adipocytes by dissipating the proton gradient before it can be used for OXPHOS (74), which results in physiologically important heat production. The role of the other four homologs of UCP1 remained elusive for a long time and is still partly undiscovered. While UCP2 is ubiquitously expressed, UCP3 is mainly found in skeletal muscle and the heart, and UCP4 as well as UCP5, also known as brain mitochondrial carrier protein-1 (BMCP1), occurred to be brain-specific (75). Although UCP2 and UCP3 are known to transport back protons into the matrix of isolated mitochondria, the evidence for heat production is still lacking (76). Moreover, these two proteins are also abundant in organisms not requiring thermogenesis such as ectothermic fish and plants. The contribution in several cellular processes was discussed in the last

years, including the possible regulation of hormone secretion (77) as well as the inhibition of inflammation and cell death by UCP2 (78) and the role of UCP3 in glucose and fatty acid transport and metabolism (79, 80). In 2007, overexpression and knockdown of UCP2 and UCP3 proteins clearly demonstrated that these proteins are essentially involved in mitochondrial Ca^{2+} uptake in response to cell stimulation. This hypothesis was further strengthened by the observation that UCP2-/- mice were lacking ruthenium red-sensitive Ca^{2+} uptake (62). Nevertheless, some groups failed to find an evidence for UCP2/3's engagement in mitochondrial Ca^{2+} uptake (81, 82). Several studies by our group (64, 83, 84) or by others (85, 86) described in detail the role of UCP2 and UCP3 in order to specify the conditions under which UCP2/3 are engaged in mitochondrial Ca^{2+} uptake. The study of Waldeck-Weiermair et. al demonstrated that modification of cytosolic Ca^{2+} levels by inhibition of SERCA switches mitochondrial Ca^{2+} uptake from a UCP2/3- and MCU-dependent to a Letm1- and MCU-dependent uptake (73). Moreover, intermembrane loop 2 (IML2) of UCP2 and UCP3 was highlighted to be absolutely essential for the engagement of UCP2/3 in mitochondrial Ca^{2+} uptake (62, 84). A recent study described that UCP2 selectively regulates a MCU-dependent extra-large mitochondrial Ca^{2+} current (xl-MCC) in HeLa cells (87) and, once again, highlightend the crucial role of UCP2/3 in mitochondrial Ca^{2+} uptake. Molecular mechanisms controlling the function of UCP2 such as gene mutations, protein turn-over regulation or posttranslational modifications are still under intensive debate and investigation (88, 89). These findings are of special interest, since UCP2 was reported to be overexpressed in cancerous tissues and to be linked to tumor growth, state of metastasis and chemoresistance (90, 91).

1.3.3 MICU1: the Ca^{2+} sensing protein

In 2010, by coupling integrative genomics, physiology, and ribonucleic acid (RNA) interference screen the gene CBARA1, afterwards called MICU1, was identified as key regulator of mitochondrial Ca^{2+} uptake. It was shown that the two highly conserved Ca^{2+} sensing EF-hands at the C-terminal end are crucial for the role of the IMM protein MICU1 in high-capacity mitochondrial calcium uptake upon IP3-mediated depletion of ER Ca^{2+} stores. The data demonstrated MICU1's importance in coupling cytosolic Ca^{2+} transients and mitochondrial energy metabolism, whereas the mitochondrial membrane potential was unaltered in cells with silenced MICU1 (65). In 2012 it was reported that MICU1 functions as a gatekeeper for MCU by preventing mitochondrial Ca^{2+} uptake at low cytosolic calcium levels (< 3 µM) (92), whereas MICU1 facilitates MCU-mediated mitochondrial Ca^{2+} uptake upon higher cytosolic calcium levels. Consequently, MICU1 prevents constitutive mitochondrial Ca^{2+} accumulation under resting conditions leading to mitochondrial Ca^{2+} overload and associated cellular stress. The reported Ca^{2+} affinity of 15-20 µM of MICU1 is in concordance with the proposed model of mitochondria-ER interplay, since these cytosolic Ca^{2+} levels are reached in regions of MAMs after depletion of internal Ca^{2+} stores. Moreover, it was demonstrated that the Ca^{2+} binding EF-hands of MICU1 are required for the regulation of MCU highlighting their essential role in the Ca^{2+} sensing mechanism (92-94). The importance of MICU1 in regulating MCU under conditions with elevated risk of Ca^{2+} overload, was shown by accelerated Ca^{2+}-overload induced mitochondrial PTP opening in MICU1-deficient hepatocytes (95). The determination of the crystal structure of MICU1 in 2014 revealed that the EF-hand containing C-terminal part of MICU1 extends into the intermembrane space and helps to stabilize MICU1 as oligomer. While MICU1 occurs as hexamer under Ca^{2+} free conditions, binding of Ca^{2+} to the two EF-hands results in disaggregation into dimers. Furthermore, this elegant study showed that two Ca^{2+} ions can bind per each MICU1 molecule (96, 97). A study by our group about MICU1 rearrangement based on a live-cell imaging approach demonstrated that cytosolic/intermembrane Ca^{2+} elevations initiate reassembly of MICU1 multimers independently from the mitochondrial matrix Ca^{2+} level, mitochondrial membrane potential and the level of the expression of MCU or EMRE (98).

1.3.4 MCU: the pore-forming protein

In 2004, a previously unknown, inwardly rectifying, Ca^{2+} selective ion channel, located in the IMM, was identified by patch-clamp experiments (61). By investigating possible interaction partners of the back then newly discovered MICU1, the transmembrane protein CCDC109A was identified as the pore-forming, ruthenium-red-sensitive mitochondrial Ca^{2+} uniporter MCU. It was demonstrated that the genes of MICU1 and MCU share striking similarities in evolution, are adjacent to each other and have the same bidirectional promotor. Moreover, data indicated that the two transmembrane domains (TMDs) containing 35 kDa protein MCU is located in the IMM with both N- and C-termini facing into the mitochondrial matrix and a linker between the two TMDs extending into the IMS. Acidic residues, forming the so called “DIME” motif, within this linker are crucial for MCU`s full function (66, 67). MCU is ubiquitously expressed among different human tissues like heart (99), pancreatic beta-cells (100) and neurons (101) and also among organisms, with just few exceptions (102). In 2013, a MCU (-/-) mouse model was presented. Mitochondria of MCU (-/-) mice are not efficient in taking up Ca^{2+}, which does not affect the basal metabolism, but causes impairment in handling strenuous work (103). It has been shown that the pore-forming MCU occurs as an oligomer with itself and with its paralog MCUb, yet the stoichiometry is still unknown. MCUb works as the dominant negative form of MCU and is one of the components within the MCU complex, besides MICU1 (65), EMRE (71) and MCUR1 (68), fine tuning the mitochondrial Ca^{2+} signal (69).

1.3.5 MCUb: the dominant negative paralog of MCU

In 2013, sequence analysis of MCU revealed a related gene, CCDC109B, called mitochondrial calcium uniporter b (MCUb), whose encoded protein, located in the IMM, shows about 50% similarity with the pore-forming MCU possessing two predicted TMDs, separated by a short loop. A critical amino-acid substitution in the pore-region as well as the lacking ability to form a calcium-permeable channel in planar lipid bilayers were reported. Insertation of MCUb into oligomers caused a dominant-negative effect leading to reduced mitochondrial Ca^{2+} uptake after agonist stimulation. In line with that, the mitochondrial Ca^{2+} uptake rate in MCUb-/- cells as well as the susceptibility to mitochondrial Ca^{2+} overload was shown to be

increased. These results strengthen the hypothesis of a regulatory function of MCUb on mitochondrial Ca^{2+} uptake by negatively modulating the uniporter activity (69).

1.3.6 MICU2: the fine-tuning Ca^{2+} sensing protein

Bioinformatics revealed additional paralogs of MICU1, the two EF-hand containing mitochondrial calcium uniport 2 and 3 (MICU2 and MICU2) localized to the IMS. While the RNA expression of MICU1, MICU2 and MCU is strongly correlating across different tissues, MICU3 is mostly abundant in the CNS. It was shown that MICU1 and MICU2 are able to stabilize each other's protein expression and that they physically interact with one another (70). Another study of the same group showed that cells lacking MICU1 and MICU2 lose a normal threshold for mitochondrial Ca^{2+} uptake. Expression of MICU1 and MICU2 mutants without functional Ca^{2+} binding sites anticipated Ca^{2+} uptake providing evidence that MICU1 and MICU2 are able to disinhibit the channel after reaching a certain threshold. Furthermore, it was shown that MICU2 is dependent on MICU1 for its activity and function (104). In line with studies showing that MICU1 prevents mitochondrial Ca^{2+} uptake at low resting conditions, but facilitates mitochondrial Ca^{2+} uptake after reaching a certain threshold (92, 93), it was demonstrated that at low Ca^{2+} levels MICU2 inhibits MCU activity, while the stimulatory effect of MICU1 on MCU activity overwhelms at higher Ca^{2+} concentrations allowing the accurate response of mitochondria to cytosolic Ca^{2+} elevations. Moreover, the physical interaction between MICU1 and MICU2 by forming heterodimers via a disulfide bond was reported. All these results identified MICU2 as a genuine gatekeeper of MCU and revealed the reason for the sigmoidal mitochondrial Ca^{2+} uptake response (105).

1.3.7 EMRE: the linker between MICU1 and MCU

Analysis of the uniporter holocomplex by mass spectrometry revealed, besides MCU, MICU1 and MICU2, a metazoan-specific 10 kDa protein with a single TMD as component. This protein was called essential MCU regulator (EMRE), since it is necessary for the uniporter channel activity and its depletion causes severe defects in mitochondrial Ca^{2+} uptake. It was proposed that EMRE interacts with MICU1 and MICU2 in the IMS and with MCU oligomers in the IMM building a bridge between pore-forming MCU with Ca^{2+} sensing MICU1 and MICU2 (71). In another study EMRE-dependent regulation was described to require MICU1, MICU2 as well as cytoplasmic Ca^{2+} and to regulate MCU channel activity by sensing matrix Ca^{2+} concentration in order to protect mitochondria from Ca^{2+} depletion or overload (106).

1.3.8 MCUR1: a fine-tuner of mitochondrial Ca^{2+} uptake

In 2012, CCDC90A, called mitochondrial calcium uniporter regulator 1 (MCUR1), was described to be an essential component for MCU-dependent mitochondrial Ca^{2+} uptake. MCUR1 is an approximately 40 kDa protein of the IMM containing 2-TMD with N- and C-termini extending into the IMS and a connecting loop in the matrix. MCUR1`s binding to MCU as well as the regulation of ruthenium red-sensitive MCU-dependent mitochondrial Ca^{2+} uptake was demonstrated. MCUR1 knockdown inhibits mitochondrial Ca^{2+} uptake and disrupts the mitochondrial respiration (68). The hypothesis of MCUR1 being a component of the MCU complex was challenged by a study showing that a lack of MCUR1 caused a decrease in the mitochondrial membrane potential pointing to a more indirect involvement of MCUR1 in mitochondrial Ca^{2+} uptake, but not to a direct effect on MCU (107). In contrast to that study, MCUR1 was shown to bind not just to MCU but also to EMRE and to work as a scaffold factor for the formation of the MCU complex (108). Another function of MCUR1 in mammalian cells seems to be the elevation of the Ca^{2+} threshold for the induction of PTP opening and therefore the prevention of cell death caused by mitochondrial Ca^{2+} overload (109).

1.3.9 Others proteins involved in mitochondrial Ca^{2+} uptake

Besides the components and regulators of the uniporter complex various, other proteins have been described to participate in several types of mitochondrial Ca^{2+} uptake. Since downregulation of MCU does not completely abolish mitochondrial Ca^{2+} uptake (66, 67), the existence of other mitochondrial Ca^{2+} uptake routes is further investigated.

Leucine zipper EF hand-containing transmembrane protein 1 (Letm1) was identified as Ca^{2+}/H^{+} exchanger of the IMM (63, 110). Letm1 was described to be involved in mitochondrial Ca^{2+} uptake upon external Ca^{2+} elevation, but not in mitochondrial Ca^{2+} uptake after agonist stimulated ER Ca^{2+} depletion (73). Silencing of Letm1 was, furthermore, shown to cause impaired basal mitochondrial oxygen consumption, increased reactive oxygen species production, AMPK activation, autophagy and cell cycle arrest (111).

Other studies demonstrated that the canonical transient receptor potential cation 3 (TRPC3) channel, located in the plasma membrane as well as in the IMM, is interacting with various mitochondrial proteins (112) and contributes to mitochondrial Ca^{2+} uptake, whenever the extramitochondrial Ca^{2+} level is high (113).

Another candidate possibly facilitating an alternative mitochondrial Ca^{2+} uptake route is the mitochondrial ryanodine receptor 1 (mRyR1), located in the IMM, in cardiac cells (114, 115). Reconstitution of mRyR1 into lipid bilayers caused a Ca^{2+} sensitive, large conductance (500-800 pS) channel (116) and in response to cytosolic Ca^{2+} elevations, mRyR1 accumulated Ca^{2+} into the mitochondrial matrix (114).

Another mode of Ca^{2+} uptake is performed by the rapid mode of Ca^{2+} uptake (RaM), sequestering Ca^{2+} rapidly at the beginning of Ca^{2+} pulses or transients (117, 118).

In 2009, mitochondrial Ca^{2+} current type 1 and 2 (mCa1 and mCa2) were characterized as voltage-gated mitochondrial Ca^{2+} channels with low sensitivity (119).

In 2014, the EF-hand domain containing solute carrier SLC25A23 was shown to play an important role in mitochondrial Ca^{2+} uptake (72).

1.4 Post translational modifications (PTMs) of mitochondria

After successful translation of messenger RNA (mRNA) codes into polypeptides by ribosomes, proteins may undergo various PTMs to reach full functionality and maturity. While gene sequence changes occur during evolution, but not during organismal development, covalent and enzymatic modifications of proteins, so called PTMs, allow fast adaptions and changes of proteins depending on recently emerging requirements (120). Developments in mass spectrometry (MS) methods allowed to identify numerous types of modifications including glycosylation, acetylation, succinylation, phosphorylation, ubiquitylation, and methylation (121). Mitochondrial proteins, predominantly encoded by the nuclear genome, except for 13 essential proteins of the mitochondrial respiratory complex, are synthesized and may also be post translationally modified in the cytosol, before they are imported into mitochondria. The finding of post translational modifications at mitochondrial DNA (mtDNA) encoded proteins, furthermore, demonstrates that PTMs may also take place directly in mitochondria (122). Chemical modifications on specific amino acid residues have recently emerged as powerful regulators of mitochondrial processes and mitochondria linked pathways. Numerous of these PTMs take place in mitochondria in order to ensure a sophisticated regulation of cellular processes and are, therefore, also linked to diseases. About 30% of mitochondrial proteins were demonstrated, for instance, to be acetylated, and mitochondrial hyperacetylation was linked to cardiac hypertrophy and cancer (123). Moreover, addition of acetylglucosamines to serine or threonine residues of proteins of the ETC was reported to be associated with diabetes (124). Another frequently occurring PTM of components of the ETC and enzymes involved in metabolic pathways is phosphorylation (125). Also succinylation of, besides others, isocitrate dehydrogenase, which takes part in a rate-limiting step in the TCA cycle, was demonstrated to occur (126). In addition, PTMs were also shown to regulate mitochondrial dynamics as well as apoptosis via, for instance, phosphorylation (127). These examples highlight the important role of PTMs on mitochondrial pathways. Nevertheless, intensive research with the help of recent developments in, for instance, MS is needed to understand their function in detail.

1.4.1 Protein arginine methyltransferases

Arginine methylation, carried out by protein arginine methyltransferases (PRMTs), is a very commonly found PTM and known to be involved in, among others, signal transduction and gene transcription (128). The methylation of arginines can sterically alter the binding possibilities of neighbouring proteins. Moreover, arginine methylations are recognized by methylarginine-binding domains, so called tudor domains, a conserved protein structural motif based on 50 amino acids, and are, therefore, possible binding sites. The amino acid arginine is especially favorable for interactions as its guanidino group contains five potential hydrogen bond donors (129). The various types of arginine methylation include monomethylarginine (MMA), asymmetric dimethylarginine (ADMA) and symmetric dimethylarginine (SDMA), and are achieved by nine different PRMTs (128), classified as either type I (PRMT1-4, -6, and -8) or type II (PRMT5, -7, and -9) according to whether they promote ADMA (type I) or SDMA (type II) after MMA (Figure 1.6).

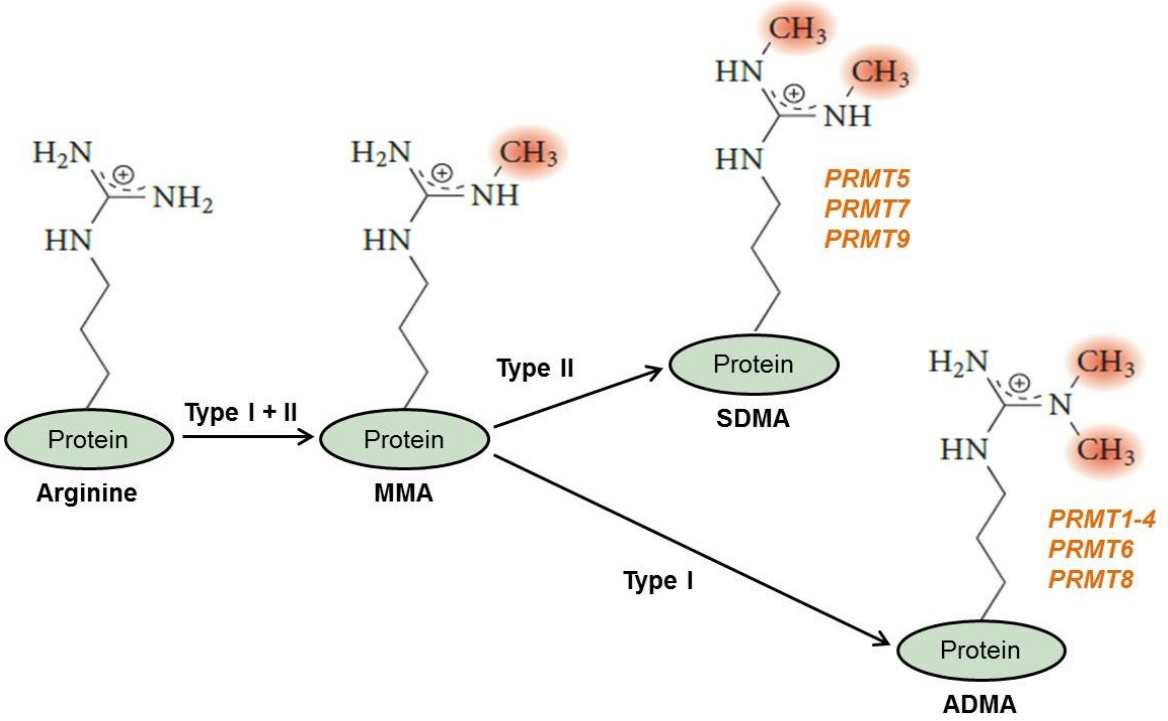

Figure 1.6: Different types of protein arginine methylation.
[modified and adopted from Yang et.al., 2013, (128)].

PRMT1, localized in nucleus and cytoplasma (130), accomplishes more than 85% of asymmetric arginine methylations and its activity is mainly linked to interactions between proteins in signal transduction pathways and cell growth (131),

but has also a key role in pathways associated with mitochondria by transferring methyl groups to arginine side chains. It was shown that PRMT1 specifically binds and methylates two arginines of B-cell lymphoma 2 (Bcl-2) antagonist of cell death (BAD) and, thereby, also modulates apoptotic processes (132). Interestingly, in was shown, that small interfering RNA (siRNA)-mediated knockdown of PRMT1 significantly decreased growth of bladder and lung cancer cells (133). In general, expression levels of PRMT1 were reported to be significantly higher in several cancer types including colon cancer (134, 135), breast cancer (136), prostate cancer (128), and lung cancer (137). Recent observations, furthermore, suggest that increased expression or activity of PRMT1 can be involved in carcinogenesis, metastasis (128) and may promote cancer cell proliferation (138).

2 OBJECTIVES OF THE STUDY

UCP2 and UCP3 were identified as crucially involved proteins in ruthenium-red-sensitive, MCU-dependent mitochondrial Ca^{2+} uptake in response to cell stimulation by our group in 2007.

This first findings were strengthened by further observations including the essential role of IML2 of UCP2 and UCP3 in the engagement of UCP2/3 in mitochondrial Ca^{2+} uptake (139) as well as the shift of mitochondrial Ca^{2+} uptake route from a UCP2/3- and MCU-dependent to a UCP2/3-independent, but MCU- and Letm1-dependent uptake via modulation of cytosolic Ca^{2+} levels by SERCA inhibition (73). Recently UCP2 was described to selectively regulate a MCU-dependent extra-large mitochondrial Ca^{2+} current (xl-MCC) in HeLa cells (87).

Nevertheless, some groups could not find any evidence for the engagement of UCP2/3 in mitochondrial Ca^{2+} uptake (81, 82).

The main aim of this study was to solve that controversy.

- *First* we looked for cells lacking UCP2/3-dependency in mitochondrial Ca^{2+} uptake. This type of mitochondrial Ca^{2+} uptake could be found in freshly-isolated human and porcine endothelial cells.
- *Second* we carefully analyzed these UCP2/3-insensitive cells in comparison to HeLa and Ea.hy926 cells, in which modulation of UCP2/3 expression strongly affects mitochondrial Ca^{2+} uptake, in order to understand, what causes UCP2/3 engagement in mitochondrial Ca^{2+} uptake.

3 MATERIALS AND METHODS

3.1 Chemicals and reagents

Cell culture materials and reagents were purchased from Greiner Bio One (Kremsmünster, Austria), chemicals for buffers and solutions from Carl Roth (Karlsruhe, Germany). Reagents and chemicals obtained from other companies are listed in Table 3.1.

Table 3.1: Supplier of reagents and chemicals.

Reagents and chemicals	
Name	**Company**
Agarose gel 1.5%	Peqlab (Erlangen, Germany)
BacMam 4mtD3cpv virus	LifeTechnologies (Vienna, Austria)
Bovine serum albumin	Sigma-Aldrich (Vienna, Austria)
Dulbecco's modified eagle medium	Sigma-Aldrich (Vienna, Austria)
EGTA	Sigma-Aldrich (Vienna, Austria)
Endothelial cell growth medium D5523	Lonza (Basel, Switzerland)
FCCP	Abcam (Cambridge, UK)
Fura-2/AM	TEFLabs (Austin, TX, USA)
Glutamine	LifeTechnologies (Vienna, Austria)
GoTaq® Green Master Mix	Promega (Mannheim, Germany)
High-capacity cDNA reverse transcription kit	Applied Biosystems (Foster City, CA, USA)
Histamine	Sigma-Aldrich (Vienna, Austria)
Human GAPDH	Qiagen (Hilden, Germany)
Fetal bovine serum	Lifetechnologies (Vienna, Austria)
Ionomycin	Abcam (Cambridge, UK)
Laemmli sample buffer (6x)	BioRad (Vienna, Austria)
Mini-PROTEAN TGX precast gels	BioRad (Vienna, Austria)
MitoTracker® Red CMXRos	Fisher Scientific (Vienna, Austria)
NuPAGE LDS sample buffer	Fisher Scientific (Vienna, Austria)
NuPAGE Sample Reducing Agent	Fisher Scientific (Vienna, Austria)
PageRulerTM Plus Prestained Protein Ladder	Fisher Scientific (Vienna, Austria)
Poly L-Lysin	Sigma-Aldrich (Vienna, Austria)

PEQLAB total RNA isolation kit	Peqlab (Erlangen, Germany)
Pierce BCA Protein Assay Kit	Fisher Scientific (Vienna, Austria)
Protease Inhibitor Cocktail	Sigma-Aldrich (Vienna, Austria)
Protein A/G plus agarose beads	Santa Cruz Biotechnology (Heidelberg, Germany)
QuantiFast SYBR Green RT-PCR kit	Qiagen (Hilden, Germany)
Rnasin® Plus Rnase inhibitor	Peqlab (Erlangen, Germany)
siRNA (different types)	Microsynth (Balgach, Switzerland)
Super signal west pico luminol/enhancer developing solution	Fisher Scientific (Vienna, Austria)
TransFast™ transfection reagent	Promega (Mannheim, Germany)

3.2 Cell culture

3.2.1 Cell harvesting and culture

HeLa and EA.hy926 cells were grown in Dulbecco's Modified Eagle Medium (DMEM) supplemented with 10% fetal bovine serum (FBS), 100 U/ml penicillin and 100 µg/ml streptomycin, as well as 2 mM glutamine, further on denoted as full DMEM. Porcine aortic endothelial cells (PAECs) were harvested by scraping cells from aortas of 3 month old piglets, kindly provided by Les Laboratoires Servier (Suresnes, France), and cultured in full DMEM. Human umbilical vein endothelial cells (HUVECs) were isolated from umbilical veins by scraping and afterwards cultured in endothelial cell growth medium (EGM-2). Freshly isolated HUVECs were kindly provided by Dr. Nicole A. Hofmann (Institute of Experimental and Clinical Pharmacology, Medical University of Graz) and Prof. Dr. Dirk Strunk (Institute of Experimental and Clinical Cell Therapy, Paracelsus Medical University Salzburg). For imaging experiments, HeLa or Ea.hy926 cells at passage 50 - 70 as well as PAECs or HUVECs at passage 1 were plated on glass coverslips (Ø = 30 mm) in 6-well plates. For other experiments, cells were grown on 10 cm cell culture dishes.

3.2.2 Ethics statement

Prior to experiments, approval was obtained for human cell and tissue sample collection from the Institutional Review Board of the Medical University of Graz (protocols 19-252 ex 07/08, 18-243 ex 06/07, 21.060 ex 09/10). Umbilical cord samples were collected after written informed consent by the mothers after full-term pregnancies in accordance with the Declaration of Helsinki.

3.2.3 Transfection procedure

Cells were transfected at a confluence between 60 – 80%, 24 h after seeding of cells on glass coverslips in 6-well plates or on 10 cm dishes. HeLa and Ea.hy926 were transfected with 1.5 µg plasmid DNA encoding the appropriate sensor alone or with 100 µM of appropriate small interfering RNA (siRNA, Table 3.2) using 2.5 µl of TransFast™ transfection reagent in 1 ml of serum- and antibiotic-free DMEM. After adding all the components the transfection mixture was briefly vortexed and incubated for 20 min at room temperature to allow cationic liposome formation. Cells were washed twice with phosphate-buffered saline (PBS) solution (Table 3.3), before transfection mixture was added. After 6 hours of incubation in a humidified incubator (37°C, 5% CO_2, 95% air) the transfection mixture was replaced by full DMEM. All experiments were performed 48 hours after transfection.

Table 3.2: Sequences of different siRNAs.

siRNA sequences	
Type	**Sequence**
human UCP2	5’ GCA CCG UCA AUG CCU ACA A dTdT 3’
human UCP3	5’ GGA ACU UUG CCC AAC AUC A dTdT 3’
human PRMT1	5’ CGU CAA AGC CAA CAA GUU A dTdT 3’
human MCU-1	5’ GCC AGA GAC AGA CAA UAC U dTdT 3’
human MCU-2	5’ GGA AAG GGA GCU UAU UGA A dTdT 3’
sus UCP2	5’ UGU CGC UCG UAA UGC CAU U dTdT 3’

For imaging experiments HUVECs and PAECs were seeded on Poly-L-Lysine coated glass coverslips in 6-well plates. These cells were transiently transfected with 100 µM of appropriate siRNA (Table 3.2) and/or 1.5 µg plasmid using 2.5 µl of TransFast™ transfection reagent according to the protocol described above.

For Ca^{2+} imaging experiments, BacMam 4mtD3cpv virus was added to full DMEM, used to replace the transfection mixture after 6 h of incubation. The amount of BacMam 4mtD3cpv virus was calculated according to the following formula:

$$\mathrm{V\ [ml]} = \frac{number\ of\ cells * 30}{1 * 10\text{^}8}$$

All experiments were performed 48 hours after transfection and infection.

Table 3.3: Composition of PBS buffer.

PBS buffer	
Components	**Conc. [mM]**
NaCl	137
KCl	2.7
Na_2HPO_4	10
KH_2PO_4	1.8

3.3 Life cell imaging

3.3.1 Measurements of mitochondrial Ca^{2+} and ER Ca^{2+}

Dynamic changes of $[Ca^{2+}]_{mito}$ and $[Ca^{2+}]_{ER}$ were followed in cells expressing genetically encoded calcium indicators (GECIs) as described in (100, 140, 141). These biosensors allow a specific targeting within living cells, a long-term expression and low toxicity. Another advantage is, that these probes are ratiometric and, therefore, the result is independent of the expression level of the sensor (142, 143). Förster resonance energy transfer (FRET) is a mechanism based on energy transfer from a donor to an acceptor chromophore, as soon as they are close enough to each other. FRET based Ca^{2+} sensors used in this study are built up by two fluorescent proteins (FPs) which are separated by calmodulin (CaM) and M13, its interacting protein from the myosine light chain kinase. Binding of Ca^{2+} to CaM initiates interaction between CaM and M13 domain causing a higher proximity between the two FPs and allowing absorbance from the emission wavelength of the donor by the acceptor (144). In our experiments 4mtD3cpv, based on cyan fluorescent protein (CFP) and circularly permuted Venus (D-cpv), as well as D1ER, built up by CFP and citrine, were used to follow dynamic changes of mitochondrial and ER Ca^{2+} levels, respectively. 48 h after transfection,

full DMEM was removed and cells were kept at room temperature in loading buffer (Table 3.4) until the measurement. During the experiments cells were perfused, according to the indicated protocol, with a Ca^{2+}-containing or with a Ca^{2+}-free buffer (Table 3.5).

Table 3.4: Composition of loading buffer.

Loading buffer	
Components	**Conc. [mM]**
$CaCl_2$	2
NaCl	135
$MgCl_2$	1
KCl	5
Hepes	10
$NaHCO_3$	2.6
KH_2PO_4	0.44
Na_2HPO_4	0.34
Glucose x $1H_20$	10
L-Glutamine	2
Amino acids	0.2%
Vitamins	0.1%
Penicillin/Streptomycin	1%
pH (adjusted with NaOH or HCl)	7.4

Table 3.5: Composition of Ca^{2+}-containing and Ca^{2+} free buffer.

Buffer:	**Ca^{2+}-containing**	**Ca^{2+}-free**
Components	**Conc. [mM]**	
$CaCl_2$	2	
NaCl	138	138
$MgCl_2$	1	1
KCl	5	5
Hepes	10	10
Glucose x $1H_20$	10	10
EGTA		0.1
pH (adjusted with NaOH or HCl)	7.4	7.4

Life cell imaging of individual cells was done on a Zeiss AxioVert inverted microscope (Zeiss; Göttingen, Germany) equipped with a polychromator illumination system (VisiChrome, Visitron Systems; Puchheim, Germany) and a thermoelectric-cooled CCD camera (Photometrics CoolSNAP HQ, Visitron Systems). Cells expressing the fluorescent Ca^{2+} biosensors were imaged with a 40× oil-immersion objective (Zeiss). Excitation of the fluorophores was at 440 ± 10 nm (440AF21, Omega Optical; Brattleboro, VT, USA), and emission was recorded at 480 and 535 nm using emission filters (480AF30 and 535AF26, Omega Optical) mounted on a Ludl filterwheel. Devices were controlled and data were acquired by VisiView 2.0.3 (Visitron Systems) software and analyzed with GraphPad Prism version 5.00 for Windows (GraphPad Software; San Diego, CA, USA). Results of FRET measurements are shown as (R_i – Background) + [(R_i – Background) - (R_0 - Background)] (where R_0 is the basal ratio) to correct for photobleaching and/or photochromism.

3.3.2 FRET-based measurements of MICU1 rearrangement

The interaction between CFP and citrine, a yellow fluorescent protein (YFP), was used to study the oligomerization of MICU1 by measuring the dynamic FRET change between MICU1-CFP and MICU1-citrine following the protocol as described by Waldeck-Weiermair et. al. (98). These measurements were performed on an inverted microscope (Axio Observer.A1, Zeiss) equipped with a polychromator illumination system (VisiChrome, Visitron Systems) and a thermoelectric-cooled CCD camera (Photometrics CoolSNAP HQ, Visitron Systems). MICU1-CFP and MICU1-citrine co-expressing HeLa cells were excited at 440 ± 10 nm (440AF21, Omega Optical), and emission was recorded at 480 and 535 nm using emission filters (480AF30 and 535AF26, Omega Optical) mounted on a Ludl filterwheel. Dissociation constants (kDs) of MICU1-MICU1 FRET reassembly were determined by the addition of various Ca^{2+} concentrations [0.1 to 1000 µM] in cells with knockdown or overexpression of certain proteins. Results of FRET measurements are presented as the ratio of F_{FRET}/F_{CFP} or as $(F_{FRET}/F_{CFP})/R_0$ (whereas R_0 is the basal ratio) to correct for photobleaching and/or photochromism.

3.3.3 Cytosolic Ca^{2+} measurements

To follow dynamical cytosolic Ca^{2+} changes, cells were incubated with the synthetic fluorescent Ca^{2+} indicator 2 µM Fura-2 acetoxymethyl ester (Fura-2/AM) in loading buffer for 30 min. After diffusion of Fura-2AM across the cell membrane, the acetoxymethyl groups are hydrolyzed by esterases and, therefore, the dye is trapped as Fura-2 in the cytosol of the cell (145). After incubation cells were washed twice with loading buffer (Table 3.4) and were then alternately illuminated at 340 and 380 nm, while fluorescence emission was recorded at 510 nm as previously described (146) on a Zeiss AxioVert inverted microscope equipped with a polychromator illumination system (VisiChrome, Visitron Systems) and a thermoelectric-cooled CCD camera (Photometrics CoolSNAP HQ, Visitron Systems). Results of Fura-2/AM measurements are shown as the ratio of F_{380}/F_{340}.

3.4 Molecular biology methods

3.4.1 RNA isolation and cDNA synthesis

Total RNA was isolated using the PEQLAB total RNA isolation kit according to the manufacturer's protocol. After washing cells twice with PBS, cells were lysed with cell lysis buffer. Cell lysates were applied on columns to remove genomic DNA. After a centrifugation step, 70% ethanol was added to the flow through and this mixture was transferred to a RNA binding column. After several centrifugation and washing steps, RNA was eluted from the column with 50 µl of nuclease-free water and the concentration of RNA was measured by using a spectrophotometer (UviLine 9400, SCHOTT Instruments; Mainz, Germany).

Reverse transcription of mRNA was performed in a thermal cycler (Peqlab) using a High-capacity cDNA reverse transcription kit from Applied Biosystems following the instructions of the manufacturer. Rnasin® Plus Rnase inhibitor was added to avoid RNA degradation. The protocol of the thermal cycler was 10 min at 25°C, 120 min at 37°C, 5 min at 85°C and in the end the temperature was kept at 4°C.

3.4.2 qRT-PCR

To control transfection efficiency or to examine the mRNA expression level of target genes under certain conditions, quantitative real-time polymerase chain reaction (qRT-PCR) was performed using QuantiFast SYBR Green RT-PCR kit on a LightCycler 480 (Roche Diagnostics; Vienna, Austria) running the following thermal cycling protocol: After initial heat activation for 5 min at 95°C, denaturation for 10 sec at 95°C, annealing as well as extension for 30 sec at 60°C (40 cycles). Data were analyzed by the REST Software (Qiagen) and relative expression of target genes was normalized to human (Table 3.1) or porcine (Table 3.6) glyceraldehyde 3-phosphate dehydrogenase (GAPDH), respectively, as a housekeeping gene. Primers, listed in Table 3.6, were designed using MS Dos Program primer designer version 2.0 and obtained from Invitrogen.

Table 3.6: Sequences of primer pairs used for qRT-PCR. h = human, s = swine

Application	Gene	Primer pair
RT-PCR	hEMRE	forward: 5'-TCGCTGGCTAGTATTGGCAC-3' reverse: 5'-GGAGAAGGCCGAAGGACATT-3'
	hMICU1	forward: 5'-CAGGTTCAGAGCATCATTCG-3' reverse: 5'-GAACACAAGCCAGACTTGAG-3'
	hMCU	forward: 5'-AGAGATAGGCTTGAGTGTGAAC-3' reverse: 5'-TTCCTGGCAGAATTTGGGAG-3'
	hMCUb	forward: 5'-TATAGTACCGTGGTGCCACCTGATG-3' reverse: 5'-TTGTAGGTCCTGAAGGAATGAACCA-3'
	hMCUR1	forward: 5'-GCAGGAGAGAGCTAAGCTTG-3' reverse: 5'-GGCATGAGTGTCGAAGTAGA-3'
	hPRMT1	forward: 5'-TGCTCAACACCGTGCTCTATGC-3' reverse: 5'-TCCTCGATGGCCGTCACATACA-3'
	hUCP2	forward: 5'-TCCTGAAAGCCAACCTCATG-3' reverse: 5'-GGCAGAGTTCATGTATCTCGTC-3'
	hUCP3	forward: 5'-AGAAAATACAGCGGGACTATGG-3' reverse: 5'-CTTGAGGATGTCGTAGGTCAC-3'
	sGAPDH	forward: 5'-TGGTGAAGGTCGGAGTGAAC-3' reverse: 5'-TGACTGTGCCGTGGAACTTG-3'

	sMCU	forward: 5'-GATAGACCTCCTTCTCCTTGACGAC-3' reverse: 5'-GTGTATAGCTGCTGGACCAGTGTCT-3'
	sMCUb	forward: 5'-TATAGTACCGTGGTGCCACCTGATG-3 reverse: 5'-TTGTAGGTCCTGAAGGAATGAACCA-3'
	sMCUR1	forward: 5'-GTCTGCCTTGGTCAAGATCACAGAG-3' reverse: 5'-TAACTGCTGAAGCGTGATCTCCTGC-3'
	sMICU1	forward: 5'-GGAGATGGAGAAGTAGACATGGAGG-3' reverse: 5'-CAAGCCAGACTTGAGGGTGTTACC-3'
	sUCP2	forward: 5'-CACTGTCGACGCCTACAAGACCATC-3' reverse: 5'-GTCATAGGTCACCAGCTCAGCACAG-3'

3.5 Proteomics

3.5.1 Cloning

For engineering MICU1 mutants (MICU1-K, MICU1-F) an already existing MICU1 plasmid was amplified with the great help of my colleague Christiane Klec via PCR with primers containing the respective mutation sequence. For both mutants the forward primer 5'-ACGGATCCATGTTTCGTCTGAACTCAC-3' with a BamHI restriction site was used. Since the mutations are very close to the end of MICU1 we decided to take a long reverse primer with an EcoRI restriction site and the following sequence:

5'-AAGAATTC-CTGTTTGGGTAAAGCGAAGTCCCAGGCAGTTTCCTGTGCACA TTTCCACATGGCCTGCATGAGXXXAGTGAAACCCAT-3', whereas XXX for mutant R455K is TTT and for mutant R455F AAA. The PCR fragment was cloned into a pcDNA3.1 (+) vector via BamHI and EcoRI sites already C-terminally containing the sequence coding for the red fluorescent protein mCherry. MICU1-CFP and MICU1-YFP were constructed following the protocol as described by Waldeck-Weiermair et. al. (98).

3.5.2 Protein isolation and quantification

48 hours after transfection cells were washed twice with PBS, scraped from 10 cm dishes, lysed with radioimmunoprecipitation assay (RIPA) buffer (Table 3.7) supplemented with Protease Inhibitor Cocktail (20 µl of Protease Inhibitor Cocktail per 1 ml RIPA buffer) and transferred into pre-cooled tubes. Cell lysates were shock frozen in liquid nitrogen for 10 sec, put on ice for 10 min and vortexed for 10 sec. This procedure was repeated 5 times. Afterwards cell lysates were centrifuged at 4000 g for 8 min at 4°C. Supernatant was collected for protein quantification. The Pierce BCA Protein Assay Kit was used according to the manufacturer's protocol. Proteins reduce Cu^{2+} to Cu^{1+} in an alkaline medium. This kit selectively detects cuprous cations by bicinchoninic acid, which results in a purple-colored reaction product. Absorbance was finally measured on a spectrophotometer (UviLine 9400, SCHOTT Instruments).

Table 3.7: Composition of RIPA buffer.

RIPA buffer	
Components	**Conc. [mM]**
Tris-HCl pH 7.6	25
NaCl	150
EDTA	5
NP-40	1%
Triton X-100	1%
Sodium deoxycholate	1%
SDS	0.1%

3.5.3 Immunoprecipitation

Protein A/G plus agarose beads (Santa Cruz) were washed with immunoprecipitation (IP)-washing buffer (Table 3.8) and incubated with 1 µg anti-flag antibody to detect flag-tagged proteins (Table 3.12) for 2 h at 4°C. Protein lysates were added and incubated with coated beads overnight at 4°C on a shaker. After three washing cycles with IP-washing buffer, NuPAGE LDS sample buffer, 1 µl of NuPAGE Sample Reducing Agent was added to the beads-lysate mix, heated for 10 min at 70°C, centrifuged with 4000 g and afterwards directly loaded onto an SDS-Page gel.

Table 3.8: Composition of IP washing buffer.

IP washing buffer	
Component	**Conc. [mM]**
Tris	10
EDTA	1
EGTA	1
NaCl	150
Na_3VO_4	0.2
Triton X-100	1%

3.5.4 Western blot

Samples were heat denatured in Laemmli sample buffer and a maximum of 40 µg for total protein lysates and 10 – 30 µl for IP samples as well as PageRulerTM Plus Prestained Protein Ladder as standard for protein size were loaded on a Mini-PROTEAN TGX precast gels, put in an electrophoresis chamber (120 V, 60 min) filled with electrophoresis buffer (100 ml of electrophoresis buffer (10x), Table 3.9, + 900 ml H_2O) and connected to the power supply Power Pack P25 (120 V, 60 min) from Biometra (Göttingen, Germany).

Table 3.9: Composition of electrophoresis buffer (10x).

Electrophoresis buffer (10x)	
Component	**Quantity [g]**
Tris base	30
Glycin	144
SDS	10
H_2O	Ad 1 l

Afterwards, gel was put in a pool filled with transfer buffer (100 ml of Tris-glycin buffer (10x), Table 3.10, + 200 ml Methanol + 700 ml H_20) and a sandwich out of a sponge, filter paper, gel, PVDF-membrane, filter paper and another sponge was made within a transfer cassette.

Table 3.9: Composition of Tris-glycin buffer (10x).

Tris-glycin buffer (10x)	
Component	**Quantity [g]**
Tris base	30.3
Glycin	144.1
20% SDS solution	5 ml
H_2O	Ad 1000 ml

The cassette was placed into the transfer chamber, filled with transfer buffer, and the chamber was connected to power supplier (400 mA, 90 min). After the transfer of proteins from the gel onto the membrane, the membrane was washed with TBS-T buffer (100 ml of TBS buffer (10x), Table 3.11, + 1 ml Tween-20 + 900 ml H_2O) and put into 5% bovine serum albumin (BSA) supplemented TBS-T buffer for one hour on a shaker.

Table 3.10: Composition of TBS buffer (10x).

TBS buffer (10x)	
Component	**Quantity [g]**
Tris base	30.3
Glycin	144.1
SDS 20% solution	5 ml
H_2O	Ad 1000 ml

This step was followed by incubation with primary antibody (Table 3.11) in TBS-T buffer overnight at 4°C. On the next day, membranes were washed one time with TBS-T buffer and were incubated twice with BSA-supplemented TBS-T buffer for 15 min. The secondary antibody (Table 3.12) was added to BSA-supplemented TBS-T buffer and the membrane was incubated for 1 hour at room temperature. After 3 washing steps with TBS-T buffer, lasting each time for 15 min, proteins were detected using super signal west pico luminol/enhancer developing solution (Fisher Scientific). Membranes were covered with detection solution, containing the substrate for the color reaction with horse radish peroxidase (HRP) labeled secondary antibodies, for 5 min and afterwards put into an envelope. Specific protein bands were visualized on a ChemiDoc MP system (BioRad).

Table 3.11: List of primary antibodies used in this study.

Primary antibodies				
Target	**Number**	**Company**	**Dilution**	**Source**
MICU1	sc-160210	Santa Cruz Biotechnology (Heidelberg, Germany)	1:200	goat
MICU1	#12524	New England Biolabs (Frankfurt, Germany)	1:1000	rabbit
MCU	#14997	New England Biolabs (Frankfurt, Germany)	1:1000	rabbit
UCP2	ab67241	Abcam (Cambridge, UK)	1:1000	mouse
Flag	F1804	Sigma-Aldrich (Vienna, Austria)	1:5000	mouse
β-actin	sc-47778	Santa Cruz Biotechnology (Heidelberg, Germany)	1:500	mouse
ADMA	#13522	New England Biolabs (Frankfurt, Germany)	1:1000	rabbit
MDMA	ab412	Abcam (Cambridge, UK)	1:1000	mouse

Table 3.12: List of secondary antibodies used in this study.

Secondary antibodies				
Target	**Number**	**Company**	**Dilution**	**Source**
anti-mouse	PI-2000	Vector Laboratories (Burlingame, CA, USA)	1:1000	horse
anti-rabbit	PI-1000	Vector Laboratories (Burlingame, CA, USA)	1:1000	goat
anti-goat	sc-2020	Santa Cruz Biotechnology (Heidelberg, Germany)	1:4000	donkey
VeriBlot	ab131366	Abcam (Cambridge, UK)	1:250	synthetic

3.6 Statistics

All experiments were performed at least three times with Ea.hy926 and HeLa. For experiments with primary cells, HUVECs and PAECs, not less than three different donors were used. For life cell imaging, numbers indicate the numbers of cells/independent repeats.

Data were processed in Microsoft Excel 2010® (Microsoft Corporation; Albuquerque, NM, USA) and statistical analyses were performed with GraphPad Prism version 5.00 for Windows (GraphPad Software; San Diego, CA, USA) by using the unpaired Student's t-test, and $p<0.05$ was considered to be significant. Data shown represent the mean ± SEM.

4 RESULTS

4.1 Cell type specific role of UCP2/3 in mitochondrial Ca^{2+} uptake

While knockdown of UCP2/3 resulted in significantly reduced mitochondrial Ca^{2+} uptake upon IP3-generating agonist stimulation in cervical cancer derived HeLa cells (Figure 4.1A) (147) and Ea.hy926 cells (Figure 4.1B), established by fusing a human umbilical vein endothelial cell with a clone of human lung carcinoma (148), the mitochondrial Ca^{2+} uptake of short-term cultured human umbilical vein endothelial cells (HUVECs) (Figure 4.1C) as well as porcine aortic endothelial cells (PAECs) (Figure 4.1D) was not affected by the expression level of UCP2/3.

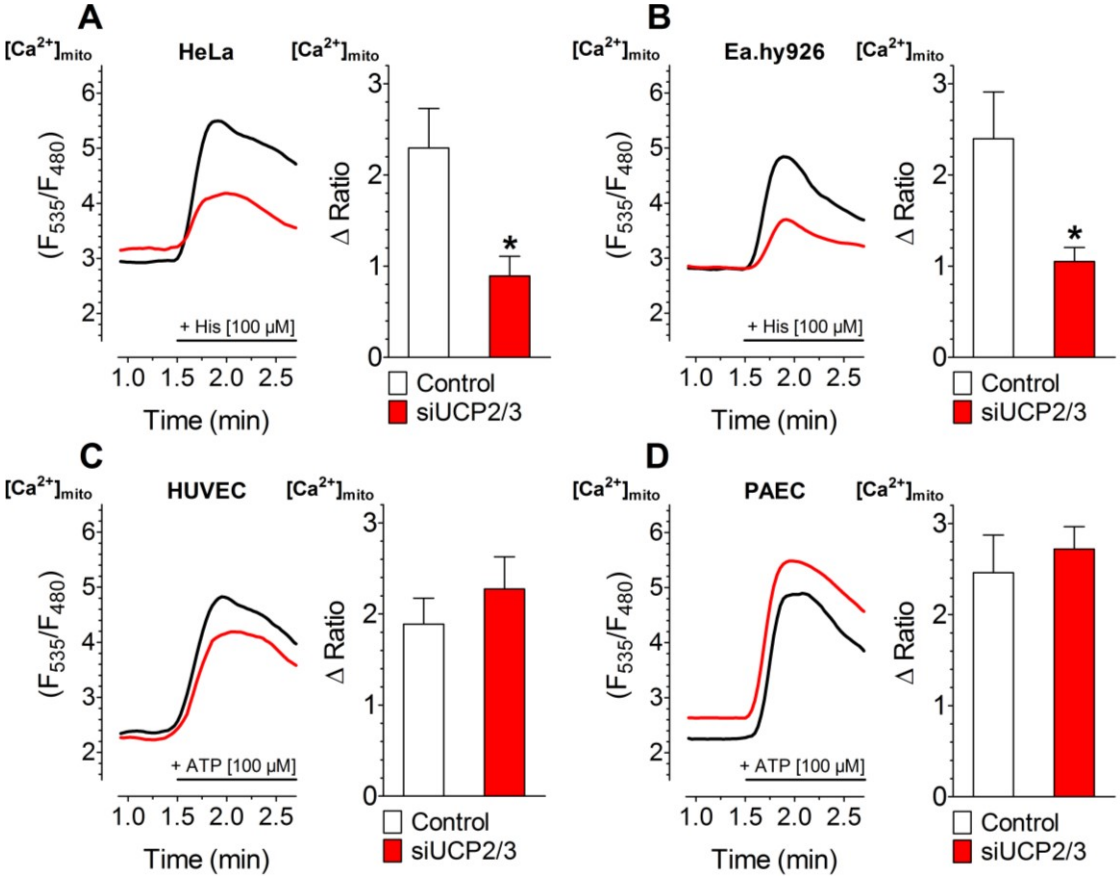

Figure 4.1: Effect of UCP2/3 knockdown on mitochondrial Ca^{2+} uptake of different cell types. *Left panels:* Representative mitochondrial Ca^{2+} ratio signals over time of 4mtD3cpv-expressing **(A)** HeLa, **(B)** Ea.hy926, **(C)** HUVEC, and **(D)** PAEC cells in response to IP3-generating agonists measured in Ca^{2+}-free solution in control cells (black curves) or cells depleted of UCP2/3 (red curves). ER Ca^{2+} release was achieved by 100 µM histamine (His) in HeLa and Ea.hy926 cells, whereas 100 µM ATP was applied as an agonist in HUVEC and PAEC cells. *Right panels:* Bars show an average of maximal Δ ratio signals (mean ± SEM) after agonist stimulation of control cells (white columns; *HeLa: n=35/13, Ea.hy926: n=29/13, HUVEC: n=37/15, and PAEC: n=17/10*) and cells with UCP2/3 knockdown (red columns; *HeLa: n=26/12, Ea.hy926: n=30/13, HUVEC: n=26/12, and PAEC: n=18/10*). n = number of cells/number of measurements. [Madreiter-Sokolowski CT et.al., Nature Communications (2016, in press)]

Notably, the transfection was successful in all four cell lines (Figure 4.2).

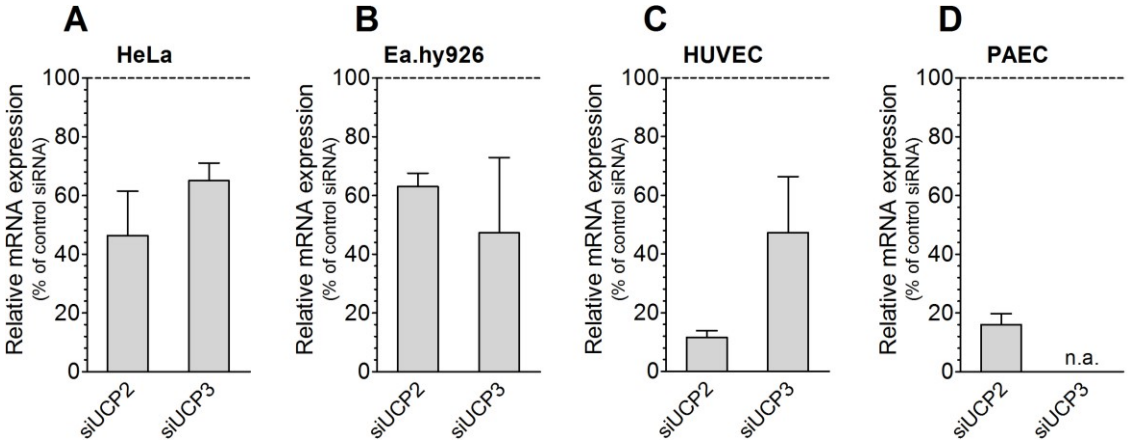

Figure 4.2: Transfection efficiency in different cell types. Bars represent an average of relative mRNA expression levels (mean ± SEM) in **(A)** HeLa, **(B)** Ea.hy926, **(C)** HUVEC, and **(D)** PAEC cells treated with siRNA against UCP2 (*n=3*) or UCP3 (*n=3*), respectively, and are normalized to mRNA expression levels of cells transfected with control siRNA (*n=3*). UCP3 mRNA was not detectable in PAEC cells. [Madreiter-Sokolowski CT et.al., Nature Communications (2016, in press)]

In contrast to UCP2/3, depletion of MCU by siRNA caused a strongly decreased mitochondrial Ca^{2+} uptake upon ER Ca^{2+} depletion in all four cell lines (Figure 4.3).

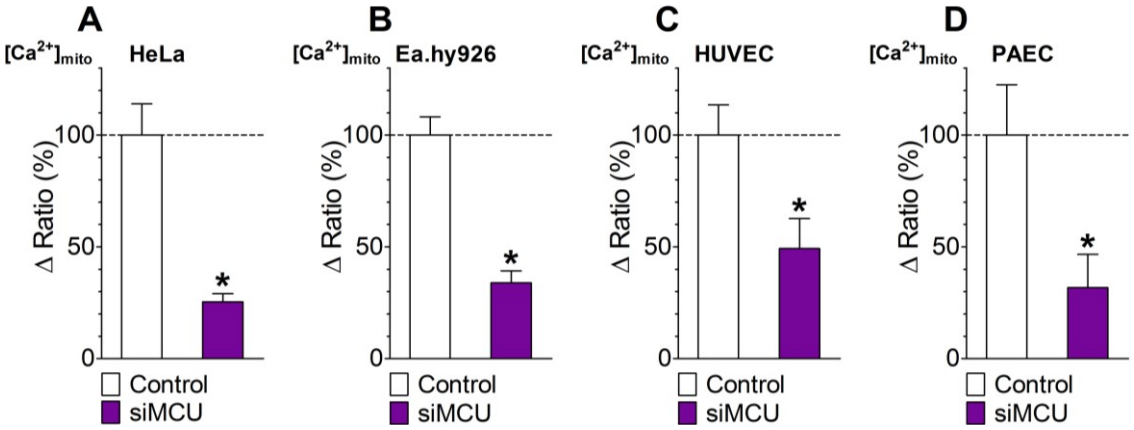

Figure 4.3: Effect of MCU knockdown on mitochondrial Ca^{2+} uptake in different cell types. Bars represent an average of maximal Δ ratio values of control cells or cells depleted of MCU after cell stimulation with histamine in **(A)** HeLa and **(B)** Ea.hy926 or with ATP in **(C)** HUVEC and **(D)** PAEC cells. Data was calculated as percentage of maximal Δ ratio values of the corresponding control (white columns; Control: *HeLa: n=32/15, Ea.hy926: n= 16/8, HUVEC: n=19/5, PAEC: n=18/11*; violet columns; siMCU: *HeLa: 37/15, Ea.hy926: 19/7, HUVEC: 24/6, PAEC: 17/10*). [Madreiter-Sokolowski CT et.al., Nature Communications (2016, in press)]

Our previous papers, already, demonstrated that UCP2/3`s effect is independent from SERCA activity, mitochondrial membrane potential and the activity of NCLX (62), pointing to a direct impact of UCP2/3 on the mitochondrial Ca^{2+} uptake machinery in HeLa and Ea.hy926.

Since the expression pattern of the core components of the MCU complex was comparable between all four cell lines (Figure 4.4), we assumed that PTMs of one

of the involved proteins might be the reason for the differences in the UCP2/3 dependency of mitochondrial Ca^{2+} uptake.

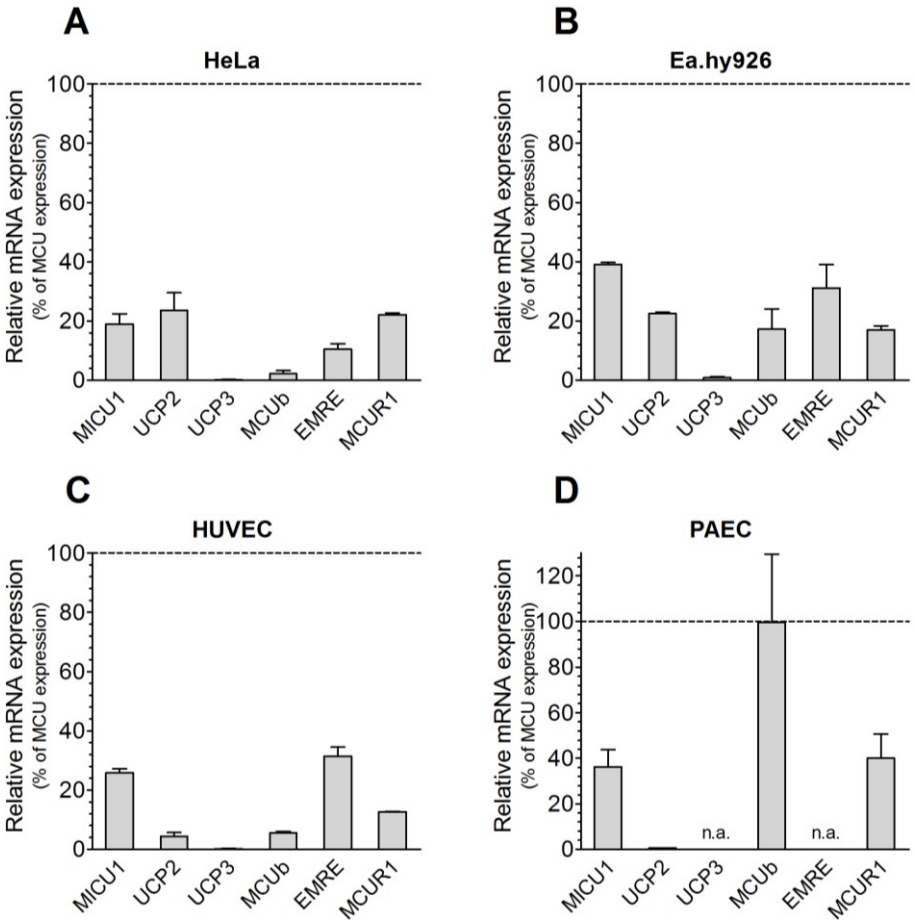

Figure 4.4: mRNA expression levels of core constituents of the MCU complex. The mRNA expression of known constituents of the MCU complex including MICU1, UCP2, UCP3, MCUb, EMRE and MCUR1 in **(A)** HeLa, **(B)** Ea.hy926, **(C)** HUVEC, and **(D)** PAEC cells, calculated as percentage of MCU mRNA expression level (*n=3*). Bar charts indicate mean ± SEM. [Madreiter-Sokolowski CT et.al., Nature Communications (2016, in press)]

4.2 PRMT1-driven methylation engages UCP2/3 in mitochondrial Ca^{2+} uptake

Because protein arginine methylation was described to be crucially involved in the regulation of numerous protein functions as well as in cell signaling pathways associated with mitochondria, we started to investigate the impact of protein arginine methylations on UCP2/3-dependency of mitochondrial Ca^{2+} uptake. Since most of the PRMTs (PRMT1-4, PRMT6, and PRMT8) are responsible for asymmetric protein dimethylation, the asymmetric arginine dimethylation state of HeLa and Ea.hy926 as well as of HUVEC and PAEC cells was analyzed by Western blot with the great help of my colleague Christiane Klec using an antibody

against asymmetric protein arginine methylation [aDMA]. The level of asymmetric protein dimethylation was remarkably higher in the immortalized HUVEC cell line Ea.hy926 than in HUVECs, the corresponding primary cells (Figure 4.5).

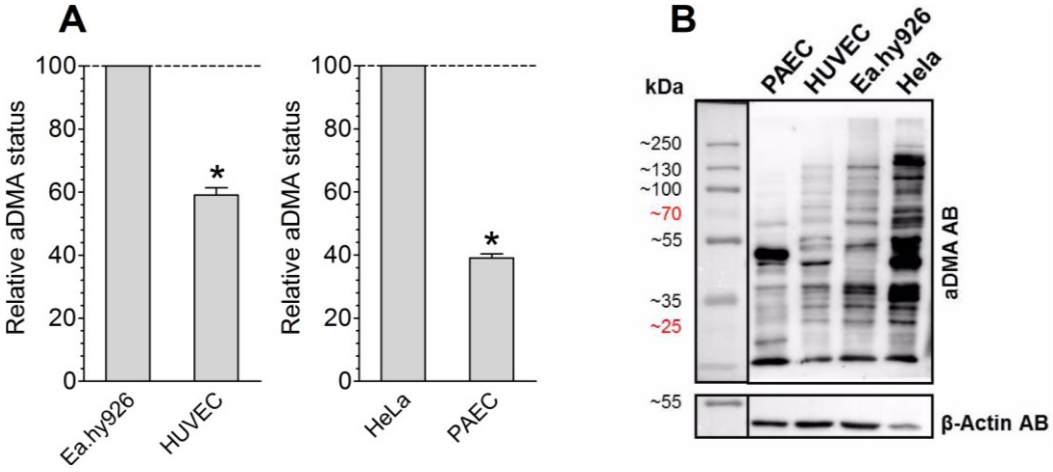

Figure 4.5: Overall asymmetric arginine dimethylation in different cell types. (A) Percentage of aDMA in HUVECs normalized to aDMA state of Ea.hy926 (*n=3*) as well as percentage of aDMA of PAECs normalized to aDMA state of HeLa (*n=4*), respectively. **(B)** Representative image of Western blot showing aDMA status of different cells by using an specific antibody against aDMA motif [aDMA] and β-actin as housekeeping gene. [Madreiter-Sokolowski CT et.al., Nature Communications (2016, in press)]

Like Ea.hy926, also HeLa cells, which are strongly dependent on UCP2/3 in mitochondrial Ca^{2+} uptake, showed a high overall state of asymmetric protein dimethylation, while the dimethylation level was significantly lower in UCP2/3-independent PAEC cells (Figure 4.5). These results gave a first hint that there is an existing correlation between the level of asymmetric protein arginine dimethylation and the UCP2/3-dependency in mitochondrial Ca^{2+} uptake. To test this hypothesis, we applied the indirect methylation inhibitor adenosine-2′,3′-dialdehyde (AdOx) and the direct PRMT inhibitor arginine n-methyltransferase inhibitor-1 (AMI-1) for 72 h, respectively, on those cell types, that had shown a clear effect in mitochondrial Ca^{2+} uptake upon UCP2/3 knockdown. AdOx is an indirect methylation inhibitor working via the inhibition of S-adenosylhomocysteine (AdoHcy) hydrolase resulting in the accumulation of intracellular AdoHcy levels (149). This causes a feedback inhibition of methylation reactions, since AdoHcy is a strong product inhibitor of S-adenosylmethionine [AdoMet], which is used by PRMTs as methyl donor (150). In contrast to the indirect methylation inhibitor AdOx, AMI-1 works as direct inhibitor of PRMT1, the most abundant PRMT (151).

Pharmacological inhibition of overall protein methylation by AdOx as well as inhibition of PRMT1-mediated protein methylation by AMI-1 were both effective (Figure 4.6A,B) and obliterated the effect of UCP2/3-knockdown on mitochondrial Ca^{2+} uptake from HeLa cells (Figure 4.6C,D), which had shown an initially UCP2/3-sensitive mitochondrial Ca^{2+} uptake.

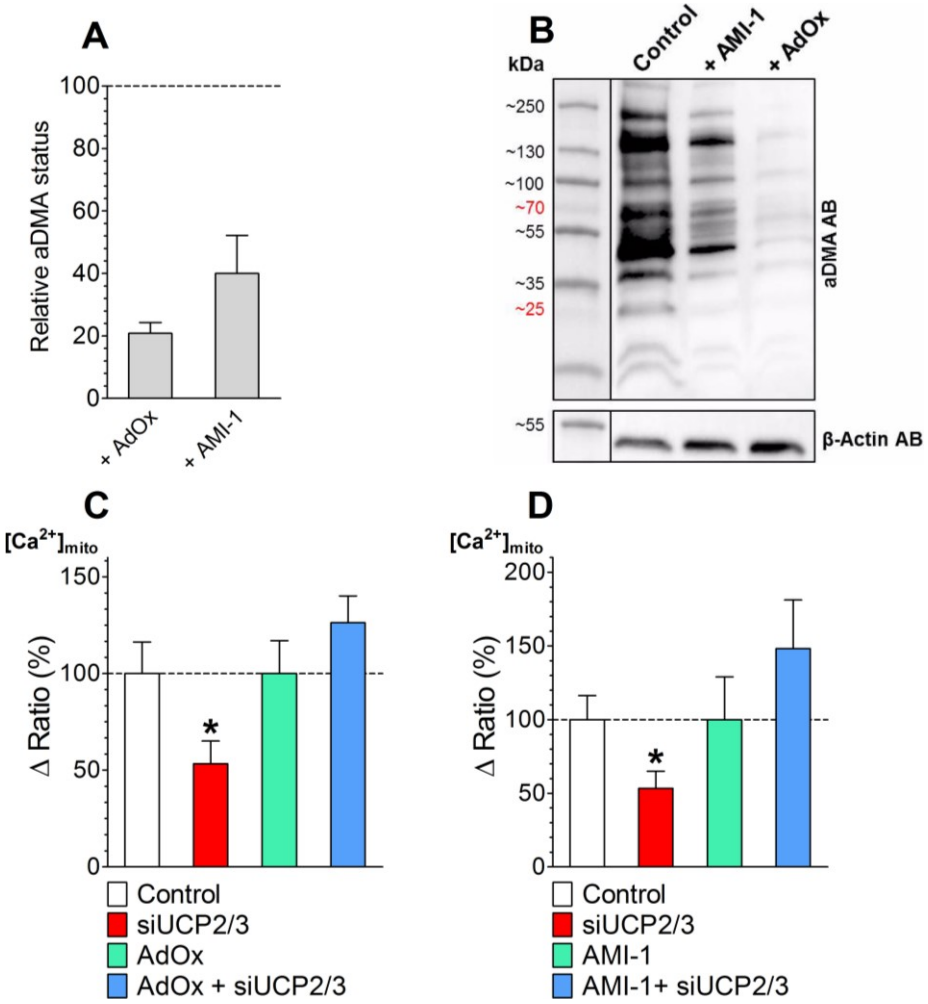

Figure 4.6: Effects of AdOx and AMI-1 on asymmetric arginine dimethylation and mitochondrial Ca^{2+} uptake. (A) Percentage of aDMA state of HeLa cells treated with 40 µM AdOx (n=7) or 5 µM AMI-1 (n=5) normalized to aDMA state of untreated HeLa cells. **(B)** Representative Western blot revealing the aDMA state by specific aDMA antibody [aDMA] and the level of housekeeping protein β-actin level of untreated HeLa or HeLa after AdOx or AMI-1 treatment. **(C)** Bars show maximal Δ ratio values in response to 100 µM histamine in Ca^{2+}-free conditions of 4mtD3cpv expressing HeLa cells treated with control siRNA (white columns: *Control: n=82/15*), siRNA against UCP2/3 (red columns; *siUCP2/3: n=80/15*), or after 72 h incubation of PRMT1 inhibitors, either 40 µM AdOx (light green columns; *AdOx: n=33/7)* or **(D)** 5 µM AMI-1 (light green columns; *AMI-1: n=66/8*), or a combination of UCP2/3 knockdown and methylation inhibitors (light blue columns; *AdOx: n=37/8, AMI-1: n=92/25*). Data was calculated as percentage of maximal Δ ratio values of HeLa cells with control siRNA (mean ± SEM). [Madreiter-Sokolowski CT et.al., Nature Communications (2016, in press)]

Next, we tested the effect of siRNA-mediated knockdown PRMTs, achieving asymmetric dimethyl arginine methylation, on the UCP2/3-dependency of mitochondrial Ca^{2+} uptake. Since PRMT8 is solely expressed in tissues of the brain, this PRMT was not tested for its effect in HeLa cells (128). While knockdown of PRMT2 (Figure 4.7C), PRMT3 (Figure 4.7D), PRMT4 (Figure 4.7E) and PRMT6 (Figure 4.7F) did not abolish the impact of UCP2/3 knockdown on mitochondrial Ca^{2+} uptake from HeLa cells (Figure 4.7A), PRMT1 depletion caused an UCP2/3-insensitive mitochondrial Ca^{2+} uptake in HeLa cells (Figure 4.7B) as well as in Ea.hy926 cells (Figure 4.8A).

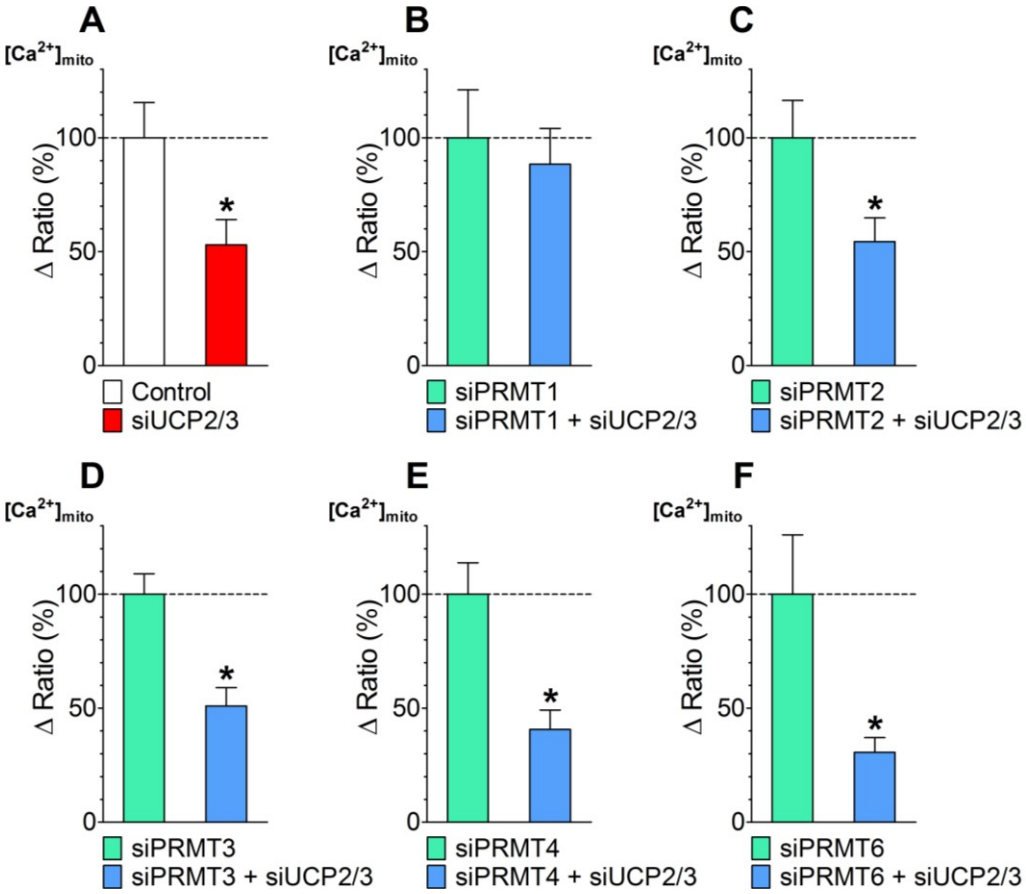

Figure 4.7: UCP2/3-dependency of mitochondrial Ca^{2+} uptake in cells depleted of different PRMTs. Bars show an average of maximal Δ ratio values in response to 100 µM histamine in Ca^{2+}-free solution of 4mtD3cpv expressing control HeLa cells or HeLa cells treated with siRNA against **(A)** PRMT1, **(B)** PRMT2, **(C)** PRMT3, **(D)** PRMT4, or **(E)** PRMT6, respectively, with or without a knockdown of UCP2/3. Data was calculated as percentage of maximal Δ ratio values of the corresponding control (white columns; *Control: n=48/6, siPRMT1: n=73/11, siPRMT2: n=86/13, siPRMT3: n=69/10, siPRMT4: n=38/11, siPRMT6: n=72/8;* red columns; *siUCP2/3: n=48/5, siPRMT1 + siUCP2/3: n=56/10, siPRMT2 + siUCP2/3: n=78/13, siPRMT3 + siUCP2/3: n=52/8, siPRMT4 + siUCP2/3: n=28/10, siPRMT6 + siUCP2/3: n=47/8*). [Madreiter-Sokolowski CT et.al., Nature Communications (2016, in press)]

The hypothesis, that PRMT1-mediated methylation engages UCP2/3 in mitochondrial Ca^{2+} uptake, was further tested by transient overexpression of PRMT1 in HUVEC cells, which exhibited no effect of UCP2/3 knockdown on mitochondrial Ca^{2+} uptake. PRMT1 overexpression, indeed, engaged UCP2/3 in mitochondrial Ca^{2+} uptake upon ER Ca^{2+} depletion in this initailly UCP2/3-insensitive cell type (Figure 4.8B).

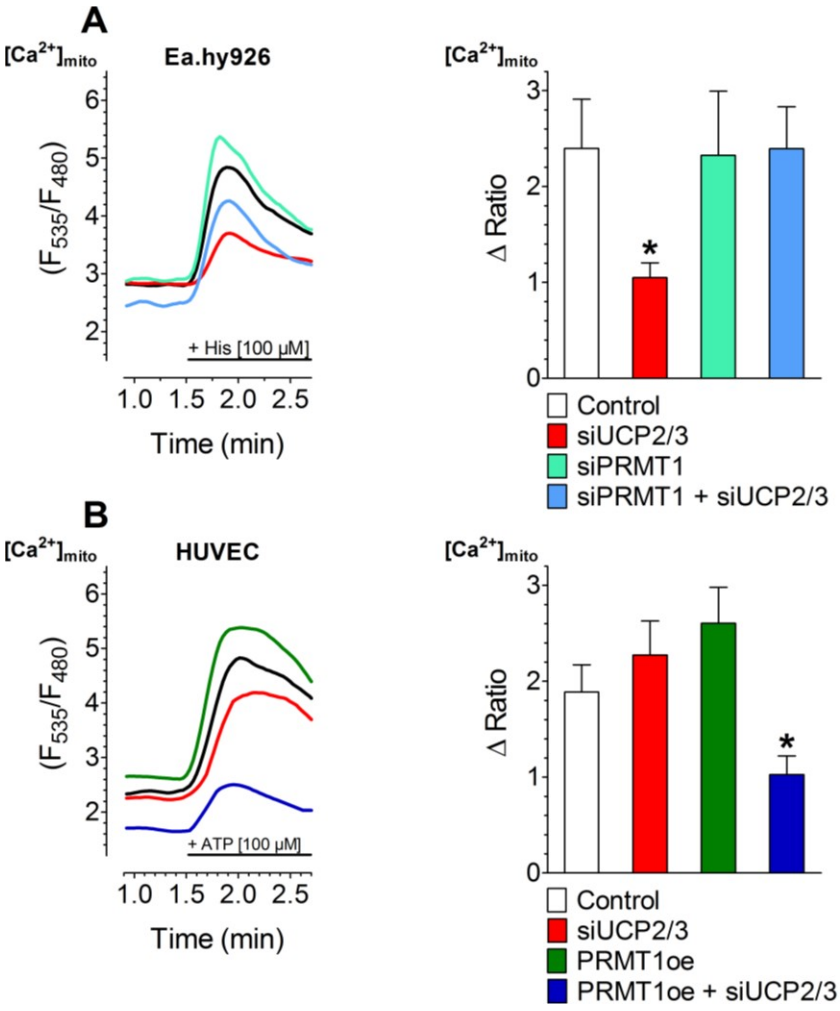

Figure 4.8: Effect of PRMT1 expression modulation on mitochondrial Ca^{2+} uptake. (A) *Left panels:* Representative curves show mitochondrial Ca^{2+} ratio signals over time of Ea.hy926 cells expressing 4mtD3cpv upon stimulation with 100 µM histamine (His) under Ca^{2+}-free conditions of control (black curves), siRNA against UCP2/3 (red curves) or PRMT1 (light green curves) or a combination of both (light blue curves). *Right panels:* Bars represent an average of maximal Δ ratio signals after exposure with an IP_3 generating agonist in cells treated with control siRNA (white columns; *n=29/13*), siUCP2/3 (red columns*; n= 30/13*), siPRMT1 (light green columns; *n=31/12*) or an combination of siUCP2/3 and siPRMT1 (light blue columns; *n=24/13*). **(B)** *Left panel:* Representative curves indicate mitochondrial Ca^{2+} ratio signals over time in response to 100 µM ATP in Ca^{2+}-free solution in HUVEC cells with control siRNA (dark curve), siRNA against UCP2/3 (red curve), overexpression of PRMT1 (dark green curve) or a combination of both (dark blue curve). *Right panel:* Bars represent an average of maximal Δ ratio signals of IP_3 agonist stimulated response of control cells (white column; *n=37/15*), cells overexpressing PRMT1 (dark green column; *n=30/12*), cells depleted of UCP2/3 (red column; *n=26/12*) or a combination of both (dark blue column; *n=38/13*). [Madreiter-Sokolowski CT et.al., Nature Communications (2016, in press)]

Neither overexpression nor knockdown of PRMT1 altered cytosolic Ca^{2+} signals (Figure 4.9A), ER Ca^{2+} content (Figure 4.9B), or basal mitochondrial Ca^{2+} concentration (Figure 4.9C).

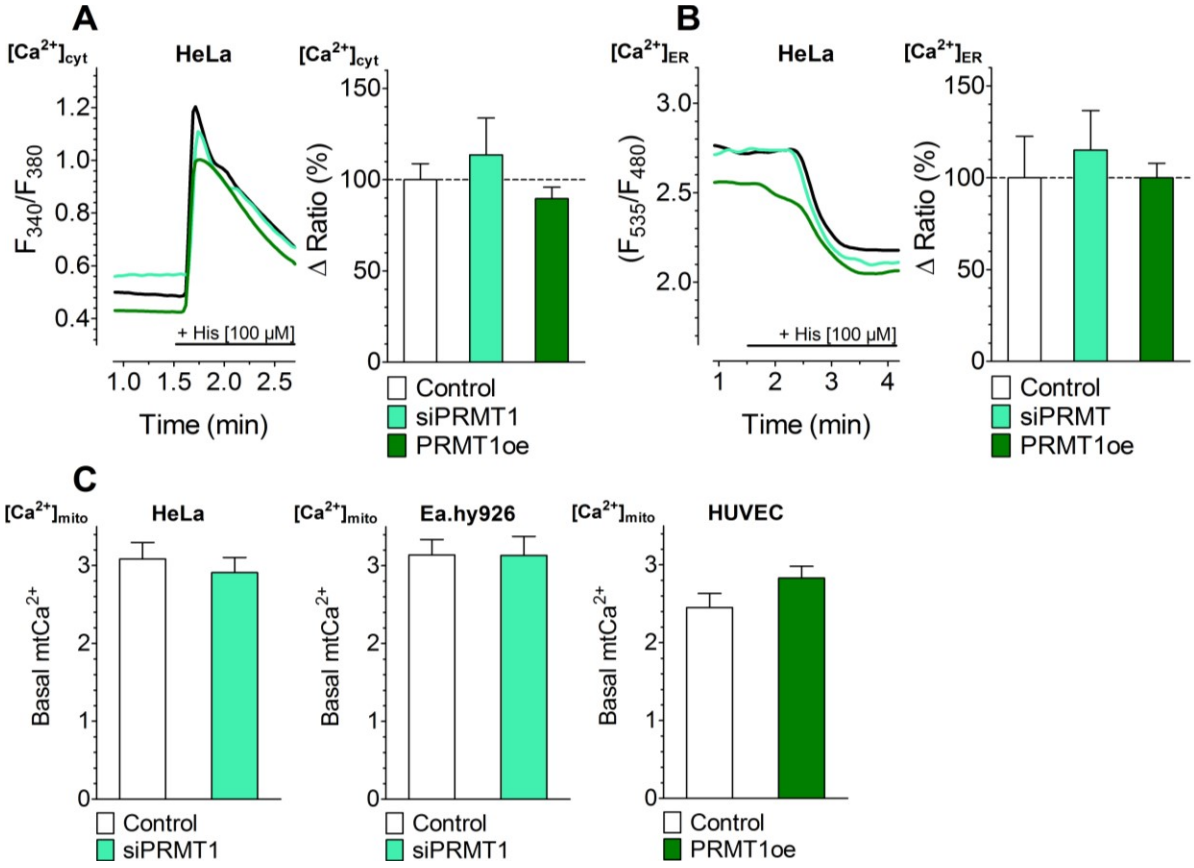

Figure 4.9: Effects of PRMT1 expression modulation on cytosolic, ER, and basal mitochondrial Ca^{2+} levels. (A) *Left panel:* Representative curves of cytosolic Ca^{2+} ratio signals over time in response to 100 µM histamine in Ca^{2+}-free solution of Fura-2/AM loaded HeLa cells treated with control siRNA (black curve), with siRNA against PRMT1 (light green curve) or Hela cells overexpressing PRMT1 (dark green curve). *Right panel:* Bars represent an average of maximal Δ ratio signals of IP_3 generating agonist treatment of control HeLa cells (white column: *n=71/9*), cells depleted of PRMT1 (light green column: *n=92/9*) or overexpressing PRMT1 (dark green column: *n=66/3*). **(B)** *Left panel:* Representative curves of $ERCa^{2+}$ ratio signals over time, measured by D1ER in HeLa cells upon stimulation with 100 µM histamine, of control HeLa cells (black curve), with either siRNA against PRMT1 (light green curve) or overexpression of PRMT1 (dark green curve). *Right panel:*Bars represent an average of maximal Δ ratio signals of IP_3 generating agonist treatment of control HeLa cells (white column: *n=25/7*), with either siRNA against PRMT1 (light green column: *n=26/8*) or overexpression of PRMT1 (dark green column: *n=12/4*). **(C)** Basal mitochondrial Ca^{2+} levels of HeLa (*left panel*) and Ea.hy926 (*middle panel*) cells with (light green columns; *HeLa: n=26/9, Ea.hy926: n=31/12*) or without knockdown of PRMT1 (white columns; *HeLa: n=35/13, Ea.hy926: n=29/13*). *Right panel:* Basal $mtCa^{2+}$ levels in control HUVEC cells (white column: *n=37/15*) or cells with PRMT1 overexpression (dark green column: *n=30/12*). Bar charts indicate mean ± SEM. [Madreiter-Sokolowski CT et.al., Nature Communications (2016, in press)]

We also analyzed the effects of PRMT1 knockdown (Figure 4.10A) or overexpression (Figure 4.10B) on the mRNA expression of core constituents of the MCU complex. Only the expression of UCP3 was altered by the modulation of PRMT1 expression. Since the expression of UCP2 is 250-fold higher than of UCP3, we assume that UCP3 plays just a minor role in that cell type (Figure 4.10C).

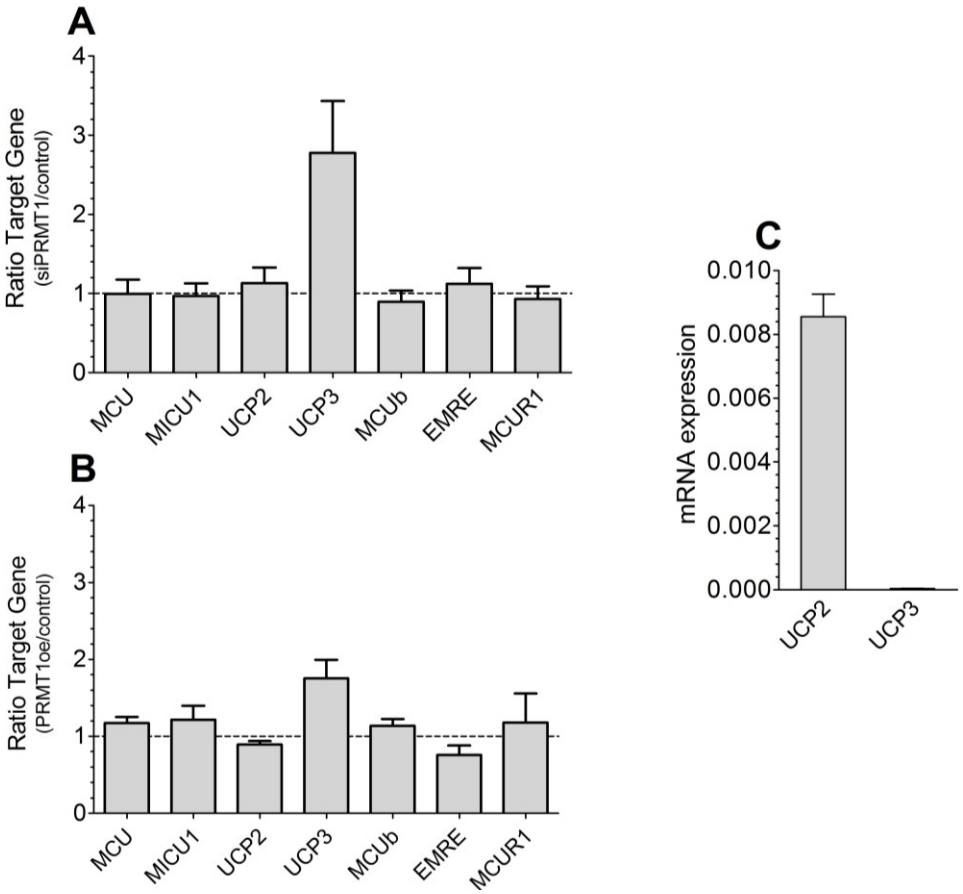

Figure 4.10: Effects of PRMT1 expression modulation on mRNA expression levels of constituents of MCU complex in HeLa cells. (A) Ratio of mRNA expression of constituents of the MCU complex including MCU, MCUb, MICU1, MCUR1, UCP2, UCP3 and EMRE in cells with knockdown of PRMT1 or **(B)** cells overexpressing PRMT1 in comparison to control cells. **(C)** Bars represent mRNA expression of UCP2 and UCP3 normalized to GAPDH as a house keeping gene *(n=3, each)*. [Madreiter-Sokolowski CT et.al., Nature Communications (2016, in press)]

In summary, all these results fit to the hypothesis, that PRMT1-mediated methylation engages UCP2/3 as fundamental regulators of MCU-dependent mitochondrial Ca^{2+} uptake.

4.3 UCP2/3 enhance Ca^{2+} sensitivity of the mitochondrial Ca^{2+} uptake machinery in case of PRMT1 activity

To understand how UCP2/3 get involved by methylation in mitochondrial Ca^{2+} uptake, the impact of PRMT1-mediated protein arginine methylation and UCP2/3 on Ca^{2+} sensitivity of mitochondrial Ca^{2+} uptake was investigated with the help of my colleagues Markus Waldeck-Weiermair and Warisara Parichatikanond in permeabilized HeLa cells with knockdown of either PRMT1 or UCP2/3 or a combined knockdown of both (Figure 4.11). The Ca^{2+} ionophore ionomycin was used to permeabilize cells and adjust different extracellular Ca^{2+} concentrations from 0 to 1000 µM. The results revealed that UCP2/3 knockdown caused a drastic loss in mitochondrial Ca^{2+} uptake sensitivity (Kd) of PRMT1-active HeLa cells from 5.3 (4.1-7.6) µM Ca^{2+} in controls to 14.1 (12.0-16.5) µM Ca^{2+} in cells depleted of UCP2/3. In contrast, siRNA against UCP2/3 did not alter Ca^{2+} sensitivity of mitochondrial Ca^{2+} sequestration in HeLa with PRMT1 knockdown (with UCP2/3: EC_{50} = 5.3 (4.1–6.8) µM Ca^{2+}, without UCP2/3: EC50 = 4.7 (3.5-6.3) µM Ca^{2+}). These results point to an enhancing function of UCP2/3 on mitochondrial Ca^{2+} machinery in case of PRMT1 activity.

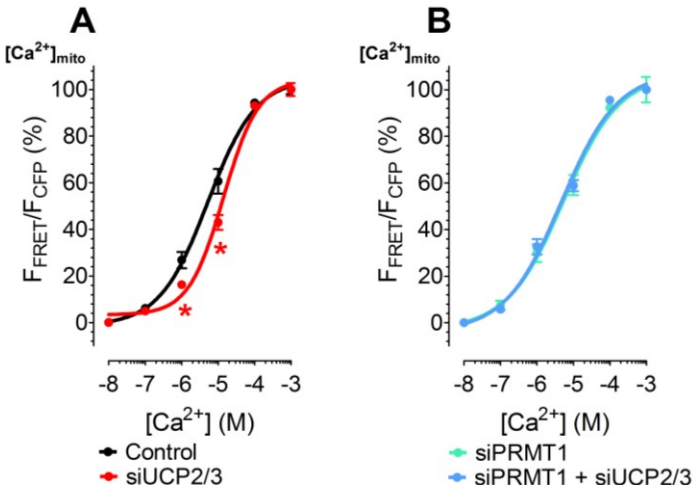

Figure 4.11: The contribution of UCP2/3 in Ca^{2+} sensitivity of mitochondrial Ca^{2+} uptake machinery. **(A)** Concentration response curves reflect mitochondrial Ca^{2+} uptake in HeLa cells with (red curve; *n=42/7*) or without (black curve; *n=16/4*) UCP2/3 knockdown treated with 3 µM of ionomycin and as indicated with different concentrations of Ca^{2+}. **(B)** Concentration response curves of mitochondrial Ca^{2+} uptake in HeLa cells with depletion of PRMT1 (light green curve; *n=28/6*) or combined depletion of PRMT1 and UCP2/3 (light blue curve*; n=24/6*) treated with 3 µM ionomycin and as indicated with different concentrations of Ca^{2+}. [Madreiter-Sokolowski CT et.al., Nature Communications (2016, in press)]

4.4 Position 455 of MICU1 is PRMT1's methylation target

The next step was to identify the methylation target of PRMT1 responsible for the changes in UCP2/3-sensitivity in mitochondrial Ca^{2+} uptake. Computational sequence analyses revealed potential methylation sites in MICU1, MCU, UCP2 and EMRE. Since the predicted methylation site of EMRE is in close proximity to the transmembrane domain, just MCU, MICU1 and UCP2 were used for further testing. Western blots using antibodies against mono- and dimethyl [MDMA] methyl as well as against asymmetric dimethyl [ADMA] protein arginine methylation, respectively, were performed. Knockdown or overexpression of PRMT1 did not affect the methylation level of MCU (Figure 4.12A) or UCP2 (Figure 4.12B), but had a strong impact on the methylation state of MICU1 (Figure 4.12C) giving a hint that MICU1 might be a target of PRMT1.

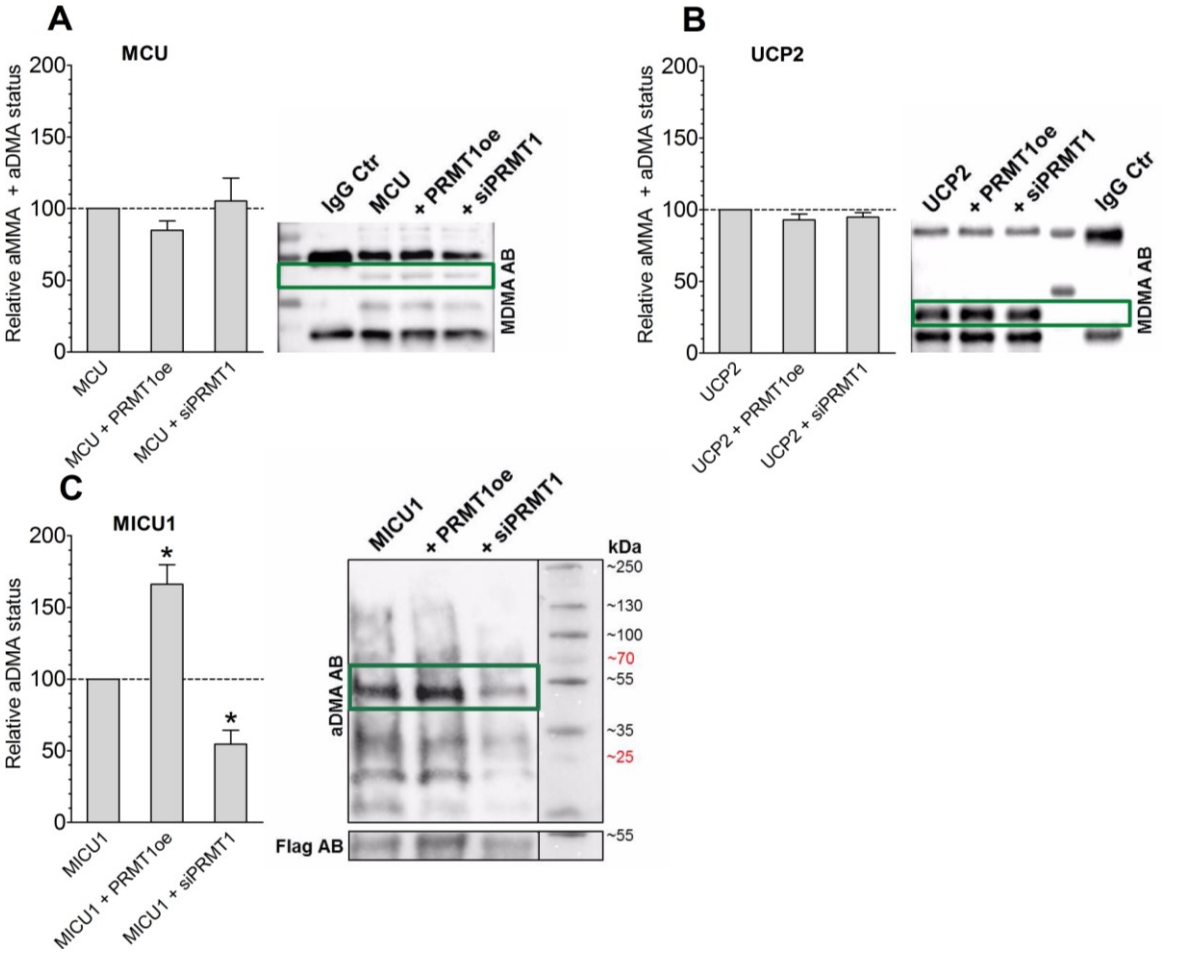

Figure 4.12: Western blots revealing methylation target of PRMT1. *Left panels:* Representative Western blots showing arginine methylation status of **(A)** MCU, **(B)** UCP2 or **(C)** MICU1, after immunoprecipitation of flag-tagged proteins, by using an antibody against mono- and dimethyl arginines [MDMA] or asymmetric dimethyl arginines [aDMA] and normalized to the intensities of detected MCU, UCP2 or Flag bands, respectively. For (A) and (B) [MDMA] antibody was used and bands were normalized to MCU or UCP2 content, respectively. For **(C)** [aDMA] antibody was used and bands were normalized to the intensity of the Flag bands. *Right panels:* Bars represent the percentage of arginine methylation of flag-tagged proteins of cells with knockdown or overexpression of PRMT1 calculated as percentage of **(A, B)** mono- and dimethyl or **(C)** asymmetric dimethyl arginine methylation of flag-tagged proteins of control cells. [Madreiter-Sokolowski CT et.al., Nature Communications (2016, in press)]

Arginine methylation at position 455 was identified as a promising candidate taking in account structural accessibility, localization in regulatory regions and sequence conservation. Position 455 is located at the C-terminus of MICU1, which is extending into the IMS and was identified to stabilize MICU1 hexamers (96). Based on hypothesis that MICU1 is methylated at position 455, a methylation mimicking MICU1 mutant, in which arginine was exchanged by a phenylalanine (MICU1-F), as well as a non-methylable MICU1, where arginine was replaced by a lysine (MICU1-K), were cloned (152). To pinpoint position 455 as methylation target of PRMT1, Western blots with wild type MICU1 and with the arginine (at position 455) lacking mutant (MICU1-K) were performed. Indeed, in contrast to wild type MICU1, the MICU1-K mutant could not be methylated by PRMT1 (Figure 4.13), showing that position 455 is the main methylation target.

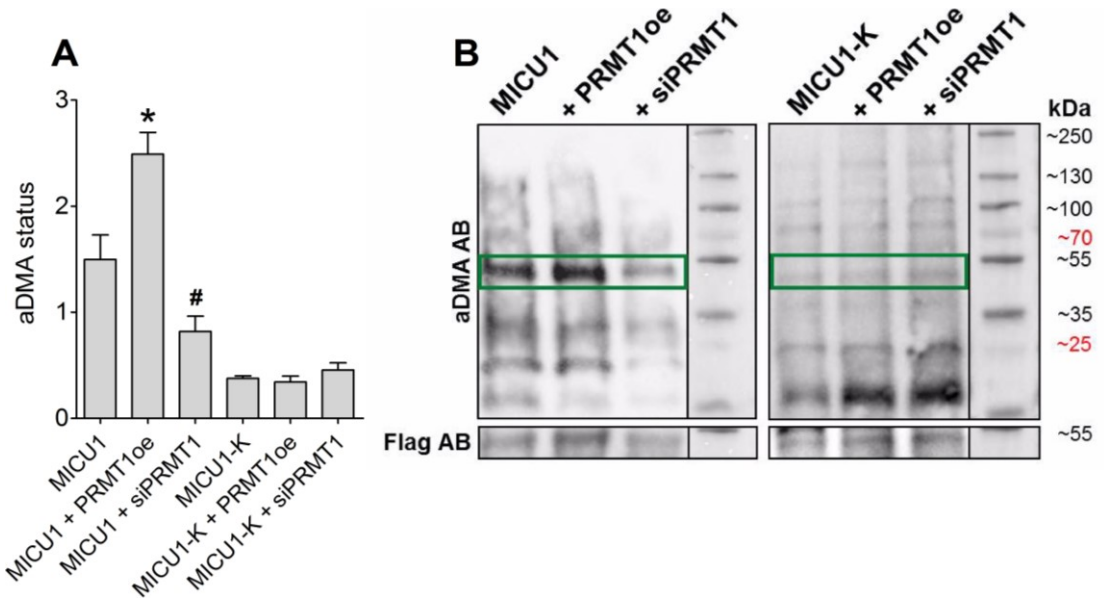

Figure 4.13: Methylation of wild type MICU1 and MICU1-K mutant. (A) Bars show aDMA status of flag-tagged wild type MICU1 or MICU1-K proteins of control cells or cells with either overexpression of knockdown of PRMT1 normalized to intensities of anti-flag bands (*n*=*3*). The statistically significant different aDMA status between wild type MICU1 and MICU1+PRMT1 was marked with a star and the statistically significant difference between wild type MICU1 and MICU1+siPRMT1 with a hash. **(B)** Representative Western blot revealing aDMA status by using [aDMA] antibody and level of anti-flag bands using a specific antibody. [Madreiter-Sokolowski CT et.al., Nature Communications (2016, in press)]

MICU-F and MICU-K mutants were also tested functionally. Therefore, MICU-K was transiently overexpressed in HeLa cells, which are exhibiting a high methylation state. In this specific cell type MICU-K mutant overexpression abolished the effect of UCP2/3-knockdown on mitochondrial Ca^{2+} uptake (Figure 4.14A). In contrast, overexpression of MICU1-F mutant in PAEC cells with low intrinsic methylation levels resulted in an UCP2/3-sensitive mitochondrial Ca^{2+} uptake (Figure 4.14B).

All these results highlight the crucial role of PRMT1-driven methylation at position 455 of MICU1 in the engagement of UCP2/3 in mitochondrial Ca^{2+} uptake.

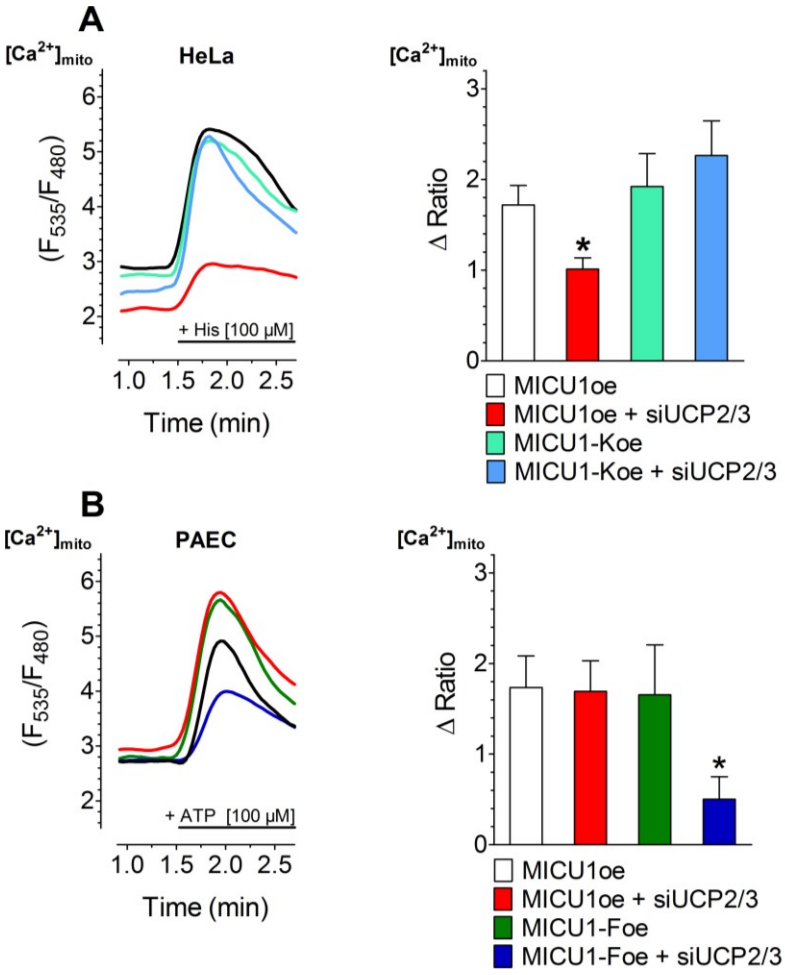

Figure 4.14: Effects of MICU1 mutants on mitochondrial Ca^{2+} uptake. (A) *Left panel:* Representative curves show mitochondrial Ca^{2+} ratio signals over time in response to 100 µM histamine in Ca^{2+}-free solution in 4mtD3cpv expressing HeLa cells overexpressing wild type MICU1 with (red curve) or without (black curve) siRNA against UCP2/3 or overexpression of MICU1-K mutant with (light blue curve) or without (light green curve) siRNA against UCP2/3. *Right panel:* Bars represent an average of maximal Δ ratio signals (mean ± SEM) of IP_3 generating agonist treatment of HeLa cells with overexpression of MICU1-WT (white column: *n=68/16*), overexpression of MICU1-WT and knockdown of UCP2/3 (red column: *n=56/18*), overexpression of MICU1-K (light green column: *n=39/16*), and combined overexpression of MICU1-K and knockdown of UCP2/3 (light blue column: *n=37/16*). **(B)** *Left panel:* Representative curves reflect mitochondrial Ca^{2+} ratio signals, measured by 4mtD3cpv, over time in response to 100 µM ATP under Ca^{2+}-free conditions of PAEC cells overexpressing wild type MICU1 treated with (red curve) or without siRNA against UCP2/3 (black curve) or PAEC cells overexpressing MICU1-F mutant with (dark blue curve) or without (dark green curve) UCP2/3. *Right panel:* Bars represent an average maximal Δ ratio signals (mean ± SEM) of IP_3 generating agonist treatment of PAEC cells overexpressing MICU1-WT (white column: *n=10/8*), overexpressing MICU1-WT and treated with siRNA against UCP2/3 (red column: *n=8/7*), overexpressing MICU1-F (dark green column: *n=13/6*) or overexpression of MICU1-F in combination with knockdown of UCP2/3 (dark blue column: *n=15/9*). [Madreiter-Sokolowski CT et.al., Nature Communications (2016, in press)]

4.5 MICU1's ability for Ca^{2+}-mediated re-arrangement is reduced by methylation and recovered by UCP2

To understand the impact of MICU1 methylation of the protein`s ability to rearrange, we performed FRET-based interaction studies in HeLa cells expressing MICU1-CFP and MICU1-YFP as previously described (98). After permeabilization with ionomycin, the concentration-response curves for Ca^{2+}-mediated reassembly of MICU1 oligomers were performed with the help of my colleague Markus Waldeck-Weiermair. While knockdown of PRMT1 did not affect Ca^{2+} sensitivity of MICU1 (Figure 4.15A), silencing of UCP2/3 caused a strong reduction in the Ca^{2+} sensitivity of MICU1 (Figure 4.15B). Remarkably, in PRMT1 depleted cells, UCP2/3 knockdown did not result in any change of MICU1's Ca^{2+} sensitivity (Figure 4.15C). Moreover, UCP2/3 knockdown was also without any effect in HeLa cells overexpressing MICU1-K mutant (Figure 4.15D).

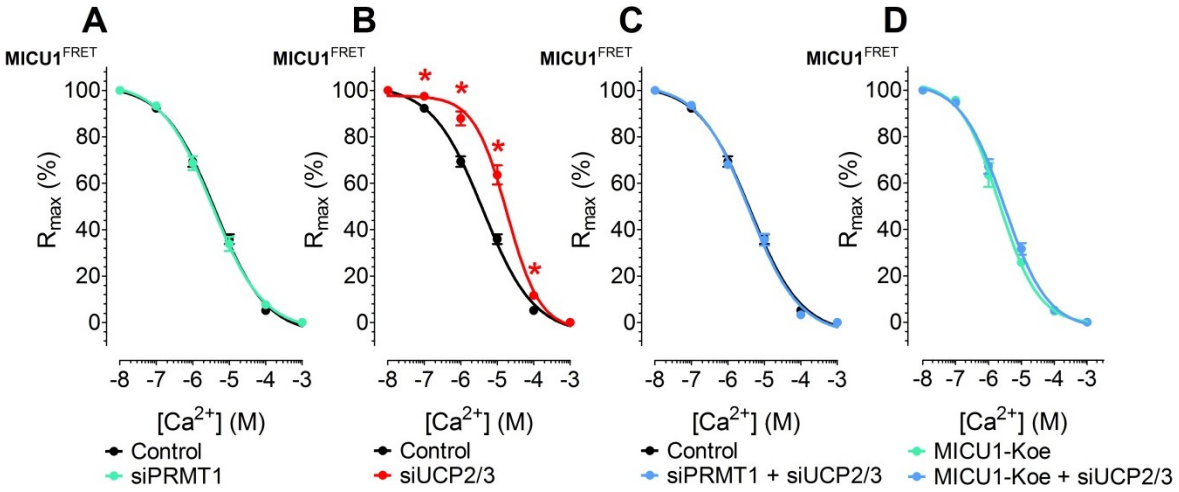

Figure 4.15: Ca^{2+} sensitivity of wild type MICU1 and MICU1-K mutant. (A) Concentration response curves of the Ca^{2+}-induced reduction of the MICU1-FRET ratio in HeLa cells treated with either control siRNA (black curve; *n=20/20*) or in combination with siRNA against PRMT1 (light green curve; *n=17/17*). Cells were treated with 3 µM ionomycin for 5 min and titrated with different concentrations of Ca^{2+}. Data express as mean ± SEM. **(B)** Concentration response curves of the Ca^{2+}-induced reduction of the MICU1-FRET ratio signal in HeLa cells with (red curve; *n=17/17*) depletion of UCP2/3 or **(C)** combined depletion of PRMT1 and UCP2/3 (light blue curve; *n=7/7*) in comparison to control siRNA (black curve; n=20/20). Cells were treated with 3 µM ionomycin and different concentrations of Ca^{2+}. **(D)** Concentration response curves of Ca^{2+}-induced reduction of MICU1-FRET ratio signal in HeLa cells overexpressing MICU1-K mutant with (light blue curve; *n=6/6*) or without (light green curve; *n=6/6*) depletion of UCP2/3. [Madreiter-Sokolowski CT et.al., Nature Communications (2016, in press)]

These results prove that PRMT1-driven methylation of MICU1 at position 455 results in a decreased Ca^{2+} sensitivity of MICU1 and, consequently, disturbs activation of MCU. Furthermore it was demonstrated, that UCP2/3 are able to re-establish the normal activity of mitochondrial Ca^{2+} uptake machinery by increasing the Ca^{2+} sensitivity of methylated MICU1.

4.6 Potential pathophysiological role of PRMT1 and UCP2 in cancer cells

While the mitochondrial Ca^{2+} uptake of somatic cells was independent of UCP2/3, a strong UCP2/3-dependency was observed in the mitochondrial Ca^{2+} uptake of the cancer cell lines HeLa and Ea.hy926 (Figure 4.1). In line with these results, also the mitochondrial Ca^{2+} uptake of the MCF-7 cells, the most studied human breast cancer cell line (153), is significantly decreased by UCP2/3 knockdown (Figure 4.16) pointing to an essential role of these proteins in the mitochondrial Ca^{2+} uptake, which may possibly ensure the energy supply in cancer cells with eleavated levels of PRMT1.

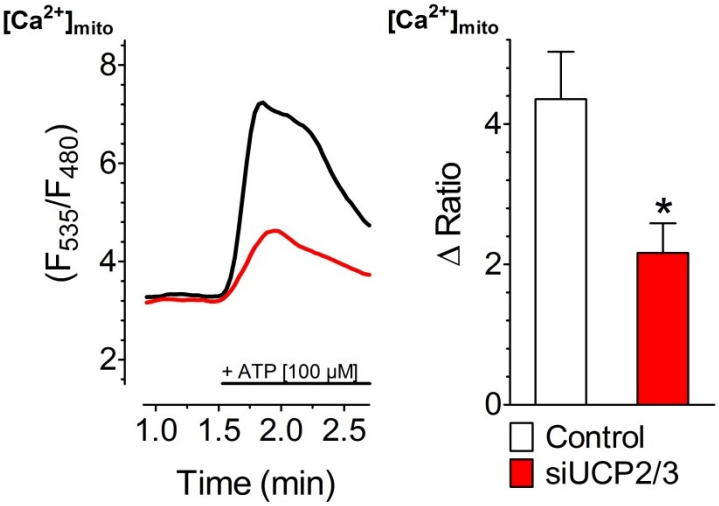

Figure 4.16: Mitochondrial Ca^{2+} uptake in MCF-7 cells. *Left panel:* Representative curves showing mtCa^{2+} ratio signals over time in response to 100 µM ATP in Ca^{2+}-free solution in MCF-7 cells with (red curve) or without (black curve) siRNA against UCP2/3. *Right panel:* Bars show maximal Δ ratio signals of IP_3 generating agonist stimulation of control cells (white column: *n=23/7*) or cells depleted of UCP2/3 (red column: *n=26/8*). [Madreiter-Sokolowski CT et.al., Nature Communications (2016, in press)]

Expression levels of PRMT1 were reported to be significantly higher in various cancer types including colon cancer (134, 135), breast cancer (136), prostate cancer (128), and lung cancer (137). Remarkably, also elevated expression levels of UCP2 were detected in several cancer types, such as breast cancer (154), colon cancer (155), pancreatic cancer, and prostate cancer (156). Similar as PRMT1, also upregulation of UCP2 was shown to be linked to tumor grade and to worse prognosis regarding the overall survival in breast cancer patients (90). To investigate that issue further, a preliminary analysis of data from The Cancer Genom Atlas (TCGA) was done with the great help of Armin Sokolowski (Department of Dentistry and Maxillofacial Surgery, Medical University of Graz).

TCGA offers comprehensive genomic profiles for selected cancer types by analyzing and sharing the data of tumor and normal tissues from hundreds of patients. The huge amount of data collected at TCGA was used to investigate the mRNA expression levels of genes coding for UCP2 and PRMT1 in breast invasive cancer, thyroid carcinoma, lung adenocarcinoma, bladder urothelial carcinoma, liver hepatocellular carcinoma, and colon adenocarcinoma tissues in comparison to corresponding adjacent healthy tissues of the same patient. Data were presented as percentage of mRNA expression and normalized to the mRNA expression of non-cancerous tissue of the same patient. TCGA analysis revealed an increase in the mRNA expression of PRMT1 as well as UCP2 in the cancer types listed in (Table 4.1).

Table 4.1: TCGA analysis of PRMT1 as well as UCP2 mRNA expression levels in different cancer types. Expression levels are presented as percentage and normalized to expression levels of non-cancerous tissues.

Cancer type	Number of cases	PRMT1 expr. [%]	UCP2 expr. [%]
Breast invasive cancer	104	131.5 ± 5.2	236.4 ± 29.2
Thyroid carcinoma	59	128.5 ± 5.0	259.5 ± 23.7
Lung adenocarcinoma	54	134.3 ± 6.8	152.6 ± 20.4
Bladder urothelial carcinoma	18	136.9 ± 10.8	359.3 ± 115.1
Liver hepatocellular carcinoma	50	137.0 ± 8.1	116.5 ± 32.0
Colorectal adenocarcinoma	26	198.5 ± 27.2	123.4 ± 22.8

5 DISCUSSION

In 2007, UCP2 and UCP3 have been demonstrated to be essentially involved in MCU-dependent mitochondrial Ca^{2+} uptake and to be independent from mitochondrial membrane potential and the activity of NCLX (62). These first findings were strengthened by showing the crucial role of UCP2/3's IML2 for the engagement of UCP2/3 in mitochondrial Ca^{2+} uptake (139). Moreover, a shift in the mitochondrial Ca^{2+} uptake route from a UCP2/3- and MCU-dependent to a UCP2/3-independent, but MCU- and Letm1-dependent uptake via modulation of cytosolic Ca^{2+} levels by SERCA inhibition could be detected (73). Notably, many studies focused on UCP2, since this isoform is widely expressed in the whole body, whereas UCP3 is mainly found in skeletal muscle (157), which was also confirmed by our results (Figure 4.10C). Recently, UCP2 was described to selectively regulate the open probability of the MCU-dependent xl-MCC in HeLa cells pointing to a regulator role of UCP2 in mitochondrial Ca^{2+} uptake (87). The important role of UCP2 in mitochondrial Ca^{2+} uptake was also confirmed by results of other groups. It was, for instance, shown that mitoplasts, which are mitochondria with an intact IMM, but missing OMM, isolated from cells of UCP2 knockout mice showed a reduced single-channel activity (158). Others revealed a crucial role of UCP2 in neurotoxicitiy by the modulation of mitochondrial Ca^{2+} levels via interaction of UCP2/3 with N-methyl-D-aspartate receptor (NMDAR) (85, 159). Notably, UCP2, which was for a long time proposed to work as moderate uncoupler of the respiratory chain similar as its well-known isoform in the brown adipose tissue, UCP1, was also clearly shown be essential for the respiratory chain without affecting reactive oxygen species (ROS) production or uncoupling (160). Nevertheless, some groups could not find any evidence for a direct engagement of UCP2/3 in mitochondrial Ca^{2+} uptake (81, 82). In this study, as depicted in Figure 5.1, we could demonstrate that PRMT1-driven methylation of MICU1 at position 455 yields reduced Ca^{2+} sensitivity of mitochondrial Ca^{2+} uptake machinery (Figure 4.11) resulting in attenuated MICU1 reassembly (Figure 4.15), which was reported to be crucial for the activity of MCU (98). In short, the PTM of MICU1 by PRMT1 causes reduced mitochondrial Ca^{2+} uptake. Under this condition the essential role of UCP2/3 could be unveiled. Our data clearly showed

that UCP2/3 works as a regulator of mitochondrial Ca^{2+} uptake in case of high PRMT1 activity by re-capturing the Ca^{2+} sensitivity of MICU1 (Figure 4.15).

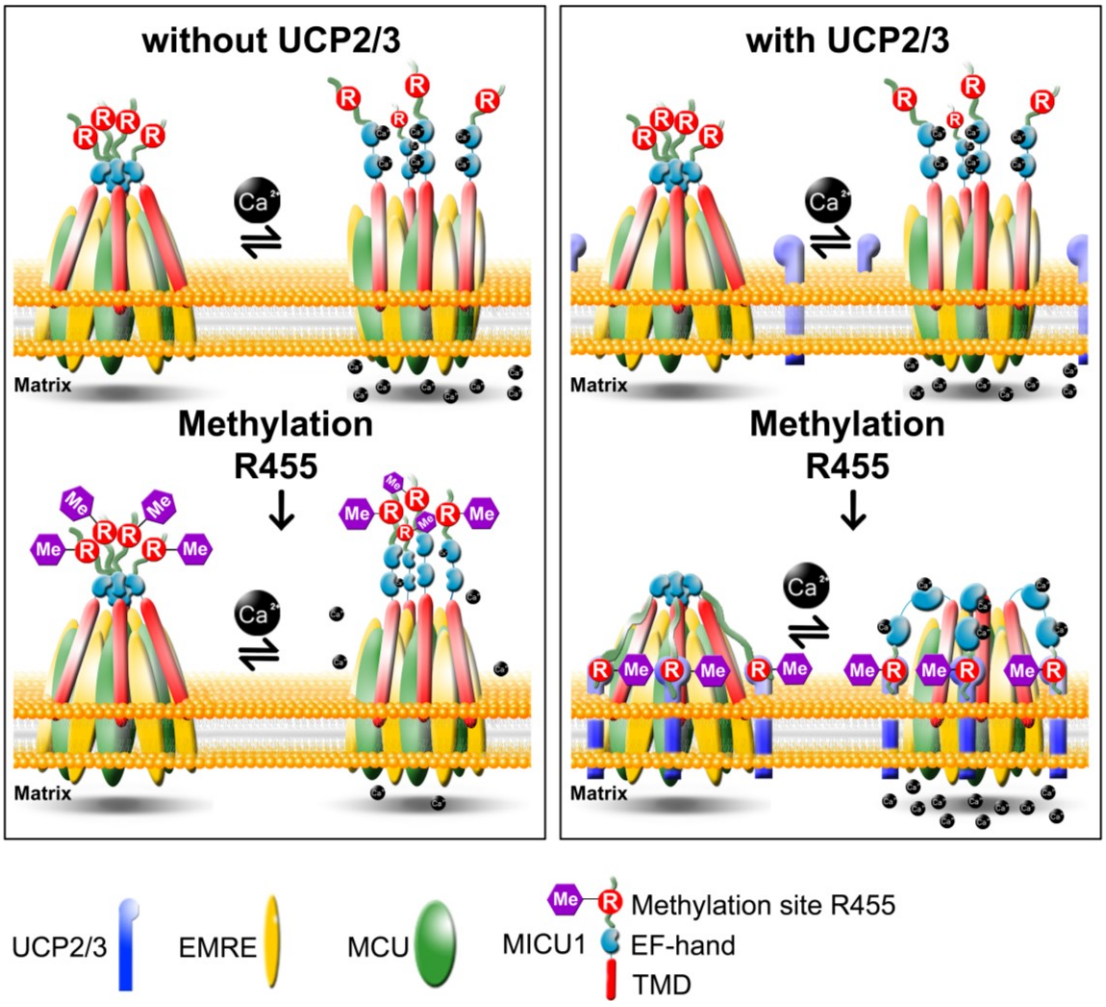

Figure 5.1: Scheme of regulatory effect of UCP2/3 in case of high PRMT1-acitivity. *Left panel:* If UCP2/3 are lacking, methylation of MICU1 at position 455 caused decreased Ca^{2+} sensitivity of MICU1 and, therefore, reduced mitochondrial Ca^{2+} uptake. *Right panel:* UCP2/3 get engaged in mitochondrial Ca^{2+} uptake in case of PRMT1-driven methylation of MICU1 and ensure proper mitochondrial Ca^{2+} uptake by increasing Ca^{2+} sensitivity of methylated MICU1.

That PRMT1-driven methylation is essential for the engagement of UCP2/3 in mitochondrial Ca^{2+} uptake was highlighted by the finding that pharmacological inhibition of overall methylation by AdOx as well as of PRMT1-mediated methylation by AMI-1 (Figure 4.6) as well as selective knockdown of PRMT1 by siRNA could prevent an effect of UCP2/3 knockdown on mitochondrial Ca^{2+} uptake of HeLa (Figure 4.7) and Ea.hy926 (Figure 4.8) cells. The knockdown of other asymmetric dimethylating PRMTs did not affect the UCP2/3-dependency of HeLa (Figure 4.7) showing that PRMT1-mediated methylation is crucial for the effect on mitochondrial Ca^{2+} uptake. This is in line with literature, since PRMT1 was described as the most abundant PRMT, which accomplishes more than 90% of arginine methylations in mammalian cells. In contrast, PRMT2, PRMT3,

PRMT4, and PRMT6 were shown to be more target-specific and PRMT8 was solely found in the central nervous system (128). Our initial finding was further strengthened by gaining UCP2/3-dependency of mitochondrial Ca^{2+} uptake in HUVECs and PAECs via overexpression of PRMT1 (Figure 4.8). Western blot results revealed that methylation of MICU1 at position 455 by PRMT1 is the key for the engagement of UCP2/3 in mitochondrial Ca^{2+} uptake, while other components of the mitochondrial Ca^{2+} uptake machinery, namely UCP2 and MCU (Figure 4.12), were not affected by PRMT1-driven methylation. Nevertheless, we can neither exclude other targets of PRMT1 within the uptake machinery nor other PTMs, which are possibly affecting the mitochondrial Ca^{2+} uptake. FRET-based Ca^{2+} measurements showed that PRMT1-mediated protein methylation caused a loss in the Ca^{2+} sensitivity of mitochondrial Ca^{2+} uptake machinery, while this effect could not be detected in cells depleted of UCP2 (Figure 4.11). Results of isothermal titration calorimetry (ITC), in press at Nature Communications (2016), confirmed these findings and revealed that methylation of MICU1 causes a reduction in the Ca^{2+} sensitivity from a dissociation constant (K_d) of 5.4 ± 0.7 µM for non-methylated MICU1 to 14.0 ± 1.5 µM binding of Ca^{2+} to methylated MICU1. To avoid improper folding of UCP2, the IML2, previously demonstrated as essential for the effect of UCP2 on mitochondrial Ca^{2+} uptake (139), was used for studying its impact on the Ca^{2+} sensitivity of purified non-methylated or methylated MICU1. Notably, IML2 was shown to solely bind to methylated MICU1 with a K_d of 24.6 ± 17.7 µM, but not to non-methylated MICU1. Moreover, IML2 shifted the Ca^{2+} sensitivity of methylated MICU1 (17.1 ± 9.9) towards that of the non-methylated MICU1 (15.4 ± 1.2) pointing to a Ca^{2+} sensitivity increasing effect of the interaction between UCP2, via IML2, and MICU1. In summary, all these data gained from different methods support the hypothesis that PRMT1-driven methylation engages UCP2/3 in order the re-establish Ca^{2+} sensitivity of methylated MICU1 and, therefore, proper mitochondrial Ca^{2+} uptake. At the beginning of this study, it was shown that the primary cells HUVECs and PAECs have an UCP2/3-independent mitochondrial Ca^{2+} uptake, while modulation of UCP2/3 expression had a strong effect in the cell lines HeLa and Ea.hy926 (Figure 4.1) as well as in MCF-7 cells (Figure 4.16). Moreover, Western blots directly compared HUVECs with Ea.hy926 cells, derived by fusing HUVECs with the permanent human lung adenocarcinoma cell line A549 (148), regarding the overall methylation state, which was significantly higher in Ea.hy926 than in

HUVECs (Figure 4.5). Interestingly, PRMT1 expression levels were reported to be significantly elevated in numerous cancer types including colon cancer (134, 135), breast cancer (136), prostate cancer (128), and lung cancer (137). Besides that also our TCGA analyses supported these findings (Table 4.1). Moreover, data of breast cancer patients revealed a better prognosis regarding the relapse free survival in case of low PRMT1 expression pattern (136). Nevertheless, the function of PRMT1 and the reason for its higher expression level in cancerous tissues is under intensive investigation and several mechanisms are discussed (128). PRMT1, for instance, was shown to crucially regulate via histone methylation the epithelial-mesenchymal transition, a process by which cell-cell adhesion of epithelial cells gets lost, which results in migration of cancer cells (161). Although more than 100 distinct types of cancer are known, cancer cells share molecular characteristics including morphological changes like disorganized arrangement and variation of size and shape as well as loss of cell cycle control resulting in limitless replication potential, tissue invasion and metastasis (162). All of these processes are linked to an increased energy demand, which is preferentially met by energy generation via glycolysis as long as glucose is available. If the availability of glucose is not assured anymore, cancer cells start to rely on alternative substrates like glutamine and mitochondria get crucially engaged in energy supply, since OXPHOS is then required to gain ATP (163). Since mitochondrial Ca^{2+} accumulation is absolutely essential for OXPHOS due to the Ca^{2+} dependency of several enzymes (164), PRMT1-driven methylation of MICU1 resulting in reduced mitochondrial Ca^{2+} uptake would strongly counteract the elevated energy demand of cancer cells. Therefore, cancer cells probably engage UCP2/3 to restore mitochondrial Ca^{2+} uptake and to ensure sufficient energy supply in cancer cells. In summary, this study helps to understand the complex role of UCP2/3 in mitochondrial Ca^{2+} uptake. It shows that UCP2/3 is absolutely essential to re-establish proper mitochondrial Ca^{2+} uptake in cells with high PRMT1 activity, which results in methylation of PRMT1 at position 455, by counteracting the attenuated Ca^{2+} sensitivity of methylated MICU1 and, therefore, normalizing mitochondrial Ca^{2+} uptake. These data unveil a novel regulation mechanism of the highyl complex mitochondrial Ca^{2+} uptake machinery. Since PRMT1 expression is increased in numerous cancer types, this study, furthermore, uncovered possible targets for novel cancer treatments.

6 REFERENCES

1. Lane N, Martin W. The energetics of genome complexity. Nature. 2010;467(7318):929-34.
2. Friedman JR, Nunnari J. Mitochondrial form and function. Nature. 2014;505(7483):335-43.
3. Neupert W, Herrmann JM. Translocation of proteins into mitochondria. Annual review of biochemistry. 2007;76:723-49.
4. Kuhlbrandt W. Structure and function of mitochondrial membrane protein complexes. BMC biology. 2015;13:89.
5. Gellerich FN, Trumbeckaite S, Opalka JR, Seppet E, Rasmussen HN, Neuhoff C, et al. Function of the mitochondrial outer membrane as a diffusion barrier in health and diseases. Biochemical Society transactions. 2000;28(2):164-9.
6. Pfanner N, Geissler A. Versatility of the mitochondrial protein import machinery. Nature reviews Molecular cell biology. 2001;2(5):339-49.
7. Zoratti M, Szabo I. Electrophysiology of the inner mitochondrial membrane. Journal of bioenergetics and biomembranes. 1994;26(5):543-53.
8. Lu YW, Claypool SM. Disorders of phospholipid metabolism: an emerging class of mitochondrial disease due to defects in nuclear genes. Frontiers in genetics. 2015;6:3.
9. Ni HM, Williams JA, Ding WX. Mitochondrial dynamics and mitochondrial quality control. Redox biology. 2015;4:6-13.
10. Kennedy EP, Lehninger AL. Oxidation of fatty acids and tricarboxylic acid cycle intermediates by isolated rat liver mitochondria. The Journal of biological chemistry. 1949;179(2):957-72.
11. Mitchell P. Coupling of phosphorylation to electron and hydrogen transfer by a chemi-osmotic type of mechanism. Nature. 1961;191:144-8.
12. Williams GS, Boyman L, Chikando AC, Khairallah RJ, Lederer WJ. Mitochondrial calcium uptake. Proceedings of the National Academy of Sciences of the United States of America. 2013;110(26):10479-86.
13. Drago I, Pizzo P, Pozzan T. After half a century mitochondrial calcium in- and efflux machineries reveal themselves. The EMBO journal. 2011;30(20):4119-25.
14. Vega-Naredo I, Loureiro R, Mesquita KA, Barbosa IA, Tavares LC, Branco AF, et al. Mitochondrial metabolism directs stemness and differentiation in P19 embryonal carcinoma stem cells. Cell Death Differ. 2014;21(10):1560-74.
15. Mandal S, Lindgren AG, Srivastava AS, Clark AT, Banerjee U. Mitochondrial function controls proliferation and early differentiation potential of embryonic stem cells. Stem cells. 2011;29(3):486-95.
16. Folmes CD, Dzeja PP, Nelson TJ, Terzic A. Mitochondria in control of cell fate. Circulation research. 2012;110(4):526-9.
17. Finkel T, Hwang PM. The Krebs cycle meets the cell cycle: mitochondria and the G1-S transition. Proceedings of the National Academy of Sciences of the United States of America. 2009;106(29):11825-6.
18. Antico Arciuch VG, Elguero ME, Poderoso JJ, Carreras MC. Mitochondrial regulation of cell cycle and proliferation. Antioxidants & redox signaling. 2012;16(10):1150-80.

19. Tait SW, Green DR. Mitochondria and cell signalling. Journal of cell science. 2012;125(Pt 4):807-15.
20. Rustin P, Kroemer G. Mitochondria and cancer. Ernst Schering Found Symp Proc. 2007(4):1-21.
21. Hockenbery DM. Targeting mitochondria for cancer therapy. Environ Mol Mutagen. 2010;51(5):476-89.
22. Griffiths EJ. Mitochondria and heart disease. Adv Exp Med Biol. 2012;942:249-67.
23. Abdallah Y, Kasseckert SA, Iraqi W, Said M, Shahzad T, Erdogan A, et al. Interplay between Ca2+ cycling and mitochondrial permeability transition pores promotes reperfusion-induced injury of cardiac myocytes. J Cell Mol Med. 2011;15(11):2478-85.
24. Kennedy BE, Madreiter CT, Vishnu N, Malli R, Graier WF, Karten B. Adaptations of energy metabolism associated with increased levels of mitochondrial cholesterol in Niemann-Pick type C1-deficient cells. The Journal of biological chemistry. 2014;289(23):16278-89.
25. de Moura MB, dos Santos LS, Van Houten B. Mitochondrial dysfunction in neurodegenerative diseases and cancer. Environ Mol Mutagen. 2010;51(5):391-405.
26. Duchen MR. Mitochondria, calcium-dependent neuronal death and neurodegenerative disease. Pflugers Archiv : European journal of physiology. 2012;464(1):111-21.
27. Rich P. Chemiosmotic coupling: The cost of living. Nature. 2003;421(6923):583.
28. Huttemann M, Lee I, Samavati L, Yu H, Doan JW. Regulation of mitochondrial oxidative phosphorylation through cell signaling. Biochimica et biophysica acta. 2007;1773(12):1701-20.
29. Naghdi S, Waldeck-Weiermair M, Fertschai I, Poteser M, Graier WF, Malli R. Mitochondrial Ca2+ uptake and not mitochondrial motility is required for STIM1-Orai1-dependent store-operated Ca2+ entry. Journal of cell science. 2010;123(Pt 15):2553-64.
30. Duchen MR. Mitochondria and calcium: from cell signalling to cell death. J Physiol. 2000;529 Pt 1:57-68.
31. Deliot N, Constantin B. Plasma membrane calcium channels in cancer: Alterations and consequences for cell proliferation and migration. Biochimica et biophysica acta. 2015;1848(10 Pt B):2512-22.
32. Brini M, Carafoli E. The plasma membrane Ca(2)+ ATPase and the plasma membrane sodium calcium exchanger cooperate in the regulation of cell calcium. Cold Spring Harbor perspectives in biology. 2011;3(2).
33. Prinz WA. Bridging the gap: membrane contact sites in signaling, metabolism, and organelle dynamics. The Journal of cell biology. 2014;205(6):759-69.
34. Raturi A, Simmen T. Where the endoplasmic reticulum and the mitochondrion tie the knot: the mitochondria-associated membrane (MAM). Biochimica et biophysica acta. 2013;1833(1):213-24.
35. Bui M, Gilady SY, Fitzsimmons RE, Benson MD, Lynes EM, Gesson K, et al. Rab32 modulates apoptosis onset and mitochondria-associated membrane (MAM) properties. The Journal of biological chemistry. 2010;285(41):31590-602.

36. Szabadkai G, Bianchi K, Varnai P, De Stefani D, Wieckowski MR, Cavagna D, et al. Chaperone-mediated coupling of endoplasmic reticulum and mitochondrial Ca2+ channels. The Journal of cell biology. 2006;175(6):901-11.
37. Merkwirth C, Langer T. Mitofusin 2 builds a bridge between ER and mitochondria. Cell. 2008;135(7):1165-7.
38. Periasamy M, Kalyanasundaram A. SERCA pump isoforms: their role in calcium transport and disease. Muscle & nerve. 2007;35(4):430-42.
39. Palty R, Silverman WF, Hershfinkel M, Caporale T, Sensi SL, Parnis J, et al. NCLX is an essential component of mitochondrial Na+/Ca2+ exchange. Proceedings of the National Academy of Sciences of the United States of America. 2010;107(1):436-41.
40. Hung CH, Ho YS, Chang RC. Modulation of mitochondrial calcium as a pharmacological target for Alzheimer's disease. Ageing research reviews. 2010;9(4):447-56.
41. Denton RM, Randle PJ, Bridges BJ, Cooper RH, Kerbey AL, Pask HT, et al. Regulation of mammalian pyruvate dehydrogenase. Mol Cell Biochem. 1975;9(1):27-53.
42. Denton RM, Richards DA, Chin JG. Calcium ions and the regulation of NAD+-linked isocitrate dehydrogenase from the mitochondria of rat heart and other tissues. The Biochemical journal. 1978;176(3):899-906.
43. Lawlis VB, Roche TE. Regulation of bovine kidney alpha-ketoglutarate dehydrogenase complex by calcium ion and adenine nucleotides. Effects on S0.5 for alpha-ketoglutarate. Biochemistry. 1981;20(9):2512-8.
44. Gerencser AA, Chinopoulos C, Birket MJ, Jastroch M, Vitelli C, Nicholls DG, et al. Quantitative measurement of mitochondrial membrane potential in cultured cells: calcium-induced de- and hyperpolarization of neuronal mitochondria. J Physiol. 2012;590(Pt 12):2845-71.
45. Racioppi L, Means AR. Calcium/calmodulin-dependent protein kinase kinase 2: roles in signaling and pathophysiology. The Journal of biological chemistry. 2012;287(38):31658-65.
46. Hausenloy DJ, Yellon DM. The mitochondrial permeability transition pore: its fundamental role in mediating cell death during ischaemia and reperfusion. J Mol Cell Cardiol. 2003;35(4):339-41.
47. Hajnoczky G, Csordas G, Das S, Garcia-Perez C, Saotome M, Sinha Roy S, et al. Mitochondrial calcium signalling and cell death: approaches for assessing the role of mitochondrial Ca2+ uptake in apoptosis. Cell calcium. 2006;40(5-6):553-60.
48. Hunter FE, Jr., Ford L. Inactivation of oxidative and phosphorylative systems in mitochondria by preincubation with phosphate and other ions. The Journal of biological chemistry. 1955;216(1):357-69.
49. Tapley DF. The effect of thyroxine and other substances on the swelling of isolated rat liver mitochondria. The Journal of biological chemistry. 1956;222(1):325-39.
50. Deluca HF, Engstrom GW. Calcium uptake by rat kidney mitochondria. Proceedings of the National Academy of Sciences of the United States of America. 1961;47:1744-50.
51. Carafoli E. The fateful encounter of mitochondria with calcium: how did it happen? Biochimica et biophysica acta. 2010;1797(6-7):595-606.

52. Moore CL. Specific inhibition of mitochondrial Ca++ transport by ruthenium red. Biochemical and biophysical research communications. 1971;42(2):298-305.
53. Moyle J, Mitchell P. Lanthanide-sensitive calcium-monocarboxylate symport in rat liver mitochondria. FEBS letters. 1977;84(1):135-40.
54. Brand MD, Chen CH, Lehninger AL. Stoichiometry of H+ ejection during respiration-dependent accumulation of Ca2+ by rat liver mitochondria. The Journal of biological chemistry. 1976;251(4):968-74.
55. Gunter TE, Gunter KK, Sheu SS, Gavin CE. Mitochondrial calcium transport: physiological and pathological relevance. The American journal of physiology. 1994;267(2 Pt 1):C313-39.
56. Santo-Domingo J, Demaurex N. Calcium uptake mechanisms of mitochondria. Biochimica et biophysica acta. 2010;1797(6-7):907-12.
57. Rizzuto R, Brini M, Pozzan T. Intracellular targeting of the photoprotein aequorin: A new approach for measuring, in living cells, Ca(2+) concentrations in defined cellular compartments. Cytotechnology. 1993;11(Suppl 1):S44-6.
58. Rizzuto R, Simpson AW, Brini M, Pozzan T. Rapid changes of mitochondrial Ca2+ revealed by specifically targeted recombinant aequorin. Nature. 1992;358(6384):325-7.
59. Rizzuto R, Pinton P, Carrington W, Fay FS, Fogarty KE, Lifshitz LM, et al. Close contacts with the endoplasmic reticulum as determinants of mitochondrial Ca2+ responses. Science. 1998;280(5370):1763-6.
60. Fontaine E, Bernardi P. Progress on the mitochondrial permeability transition pore: regulation by complex I and ubiquinone analogs. Journal of bioenergetics and biomembranes. 1999;31(4):335-45.
61. Kirichok Y, Krapivinsky G, Clapham DE. The mitochondrial calcium uniporter is a highly selective ion channel. Nature. 2004;427(6972):360-4.
62. Trenker M, Malli R, Fertschai I, Levak-Frank S, Graier WF. Uncoupling proteins 2 and 3 are fundamental for mitochondrial Ca2+ uniport. Nature cell biology. 2007;9(4):445-52.
63. Jiang D, Zhao L, Clapham DE. Genome-wide RNAi screen identifies Letm1 as a mitochondrial Ca2+/H+ antiporter. Science. 2009;326(5949):144-7.
64. Waldeck-Weiermair M, Jean-Quartier C, Rost R, Khan MJ, Vishnu N, Bondarenko AI, et al. Leucine zipper EF hand-containing transmembrane protein 1 (Letm1) and uncoupling proteins 2 and 3 (UCP2/3) contribute to two distinct mitochondrial Ca2+ uptake pathways. The Journal of biological chemistry. 2011;286(32):28444-55.
65. Perocchi F, Gohil VM, Girgis HS, Bao XR, McCombs JE, Palmer AE, et al. MICU1 encodes a mitochondrial EF hand protein required for Ca(2+) uptake. Nature. 2010;467(7313):291-6.
66. Baughman JM, Perocchi F, Girgis HS, Plovanich M, Belcher-Timme CA, Sancak Y, et al. Integrative genomics identifies MCU as an essential component of the mitochondrial calcium uniporter. Nature. 2011;476(7360):341-5.
67. De Stefani D, Raffaello A, Teardo E, Szabo I, Rizzuto R. A forty-kilodalton protein of the inner membrane is the mitochondrial calcium uniporter. Nature. 2011;476(7360):336-40.
68. Mallilankaraman K, Cardenas C, Doonan PJ, Chandramoorthy HC, Irrinki KM, Golenar T, et al. MCUR1 is an essential component of mitochondrial

Ca2+ uptake that regulates cellular metabolism. Nature cell biology. 2012;14(12):1336-43.
69. Raffaello A, De Stefani D, Sabbadin D, Teardo E, Merli G, Picard A, et al. The mitochondrial calcium uniporter is a multimer that can include a dominant-negative pore-forming subunit. The EMBO journal. 2013;32(17):2362-76.
70. Plovanich M, Bogorad RL, Sancak Y, Kamer KJ, Strittmatter L, Li AA, et al. MICU2, a paralog of MICU1, resides within the mitochondrial uniporter complex to regulate calcium handling. PloS one. 2013;8(2):e55785.
71. Sancak Y, Markhard AL, Kitami T, Kovacs-Bogdan E, Kamer KJ, Udeshi ND, et al. EMRE is an essential component of the mitochondrial calcium uniporter complex. Science. 2013;342(6164):1379-82.
72. Hoffman NE, Chandramoorthy HC, Shanmughapriya S, Zhang XQ, Vallem S, Doonan PJ, et al. SLC25A23 augments mitochondrial Ca(2)(+) uptake, interacts with MCU, and induces oxidative stress-mediated cell death. Molecular biology of the cell. 2014;25(6):936-47.
73. Waldeck-Weiermair M, Deak AT, Groschner LN, Alam MR, Jean-Quartier C, Malli R, et al. Molecularly distinct routes of mitochondrial Ca2+ uptake are activated depending on the activity of the sarco/endoplasmic reticulum Ca2+ ATPase (SERCA). The Journal of biological chemistry. 2013;288(21):15367-79.
74. Ricquier D, Bouillaud F. The uncoupling protein homologues: UCP1, UCP2, UCP3, StUCP and AtUCP. The Biochemical journal. 2000;345 Pt 2:161-79.
75. Robbins D, Zhao Y. New aspects of mitochondrial Uncoupling Proteins (UCPs) and their roles in tumorigenesis. International journal of molecular sciences. 2011;12(8):5285-93.
76. Krauss S, Zhang CY, Lowell BB. The mitochondrial uncoupling-protein homologues. Nature reviews Molecular cell biology. 2005;6(3):248-61.
77. Diao J, Allister EM, Koshkin V, Lee SC, Bhattacharjee A, Tang C, et al. UCP2 is highly expressed in pancreatic alpha-cells and influences secretion and survival. Proceedings of the National Academy of Sciences of the United States of America. 2008;105(33):12057-62.
78. Mattiasson G, Sullivan PG. The emerging functions of UCP2 in health, disease, and therapeutics. Antioxidants & redox signaling. 2006;8(1-2):1-38.
79. Schrauwen P, Hesselink MK. The role of uncoupling protein 3 in fatty acid metabolism: protection against lipotoxicity? The Proceedings of the Nutrition Society. 2004;63(2):287-92.
80. Liu J, Li J, Li WJ, Wang CM. The role of uncoupling proteins in diabetes mellitus. Journal of diabetes research. 2013;2013:585897.
81. De Marchi U, Castelbou C, Demaurex N. Uncoupling protein 3 (UCP3) modulates the activity of Sarco/endoplasmic reticulum Ca2+-ATPase (SERCA) by decreasing mitochondrial ATP production. The Journal of biological chemistry. 2011;286(37):32533-41.
82. Brookes PS, Parker N, Buckingham JA, Vidal-Puig A, Halestrap AP, Gunter TE, et al. UCPs--unlikely calcium porters. Nature cell biology. 2008;10(11):1235-7; author reply 7-40.
83. Deak AT, Jean-Quartier C, Bondarenko AI, Groschner LN, Malli R, Graier WF, et al. Assessment of mitochondrial Ca(2)(+) uptake. Methods in molecular biology. 2015;1264:421-39.

84. Waldeck-Weiermair M, Malli R, Naghdi S, Trenker M, Kahn MJ, Graier WF. The contribution of UCP2 and UCP3 to mitochondrial Ca(2+) uptake is differentially determined by the source of supplied Ca(2+). Cell calcium. 2010;47(5):433-40.
85. Fukumori R, Takarada T, Kambe Y, Nakazato R, Fujikawa K, Yoneda Y. Possible involvement of mitochondrial uncoupling protein-2 in cytotoxicity mediated by acquired N-methyl-D-aspartate receptor channels. Neurochemistry international. 2012;61(4):498-505.
86. Motloch LJ, Reda S, Wolny M, Hoppe UC. UCP2 Modulates Cardioprotective Effects of Ru360 in Isolated Cardiomyocytes during Ischemia. Pharmaceuticals. 2015;8(3):474-82.
87. Bondarenko AI, Parichatikanond W, Madreiter CT, Rost R, Waldeck-Weiermair M, Malli R, et al. UCP2 modulates single-channel properties of a MCU-dependent Ca(2+) inward current in mitochondria. Pflugers Archiv : European journal of physiology. 2015;467(12):2509-18.
88. Mailloux RJ, Seifert EL, Bouillaud F, Aguer C, Collins S, Harper ME. Glutathionylation acts as a control switch for uncoupling proteins UCP2 and UCP3. The Journal of biological chemistry. 2011;286(24):21865-75.
89. Donadelli M, Dando I, Fiorini C, Palmieri M. UCP2, a mitochondrial protein regulated at multiple levels. Cellular and molecular life sciences : CMLS. 2014;71(7):1171-90.
90. Sayeed A, Meng Z, Luciani G, Chen LC, Bennington JL, Dairkee SH. Negative regulation of UCP2 by TGFbeta signaling characterizes low and intermediate-grade primary breast cancer. Cell death & disease. 2010;1:e53.
91. Pons DG, Nadal-Serrano M, Torrens-Mas M, Valle A, Oliver J, Roca P. UCP2 inhibition sensitizes breast cancer cells to therapeutic agents by increasing oxidative stress. Free radical biology & medicine. 2015;86:67-77.
92. Mallilankaraman K, Doonan P, Cardenas C, Chandramoorthy HC, Muller M, Miller R, et al. MICU1 is an essential gatekeeper for MCU-mediated mitochondrial Ca(2+) uptake that regulates cell survival. Cell. 2012;151(3):630-44.
93. Csordas G, Golenar T, Seifert EL, Kamer KJ, Sancak Y, Perocchi F, et al. MICU1 controls both the threshold and cooperative activation of the mitochondrial Ca(2)(+) uniporter. Cell metabolism. 2013;17(6):976-87.
94. Kevin Foskett J, Madesh M. Regulation of the mitochondrial Ca(2+) uniporter by MICU1 and MICU2. Biochemical and biophysical research communications. 2014;449(4):377-83.
95. Antony AN, Paillard M, Moffat C, Juskeviciute E, Correnti J, Bolon B, et al. MICU1 regulation of mitochondrial Ca(2+) uptake dictates survival and tissue regeneration. Nature communications. 2016;7:10955.
96. Wang L, Yang X, Li S, Wang Z, Liu Y, Feng J, et al. Structural and mechanistic insights into MICU1 regulation of mitochondrial calcium uptake. The EMBO journal. 2014;33(6):594-604.
97. Tian Y, Qin L, Qiu H, Shi D, Sun R, Li W, et al. RPS3 regulates melanoma cell growth and apoptosis by targeting Cyto C/Ca2+/MICU1 dependent mitochondrial signaling. Oncotarget. 2015;6(30):29614-25.
98. Waldeck-Weiermair M, Malli R, Parichatikanond W, Gottschalk B, Madreiter-Sokolowski CT, Klec C, et al. Rearrangement of MICU1 multimers for activation of MCU is solely controlled by cytosolic Ca(2.). Scientific reports. 2015;5:15602.

99. Joiner ML, Koval OM, Li J, He BJ, Allamargot C, Gao Z, et al. CaMKII determines mitochondrial stress responses in heart. Nature. 2012;491(7423):269-73.
100. Alam MR, Groschner LN, Parichatikanond W, Kuo L, Bondarenko AI, Rost R, et al. Mitochondrial Ca2+ uptake 1 (MICU1) and mitochondrial ca2+ uniporter (MCU) contribute to metabolism-secretion coupling in clonal pancreatic beta-cells. The Journal of biological chemistry. 2012;287(41):34445-54.
101. Liao Y, Hao Y, Chen H, He Q, Yuan Z, Cheng J. Mitochondrial calcium uniporter protein MCU is involved in oxidative stress-induced cell death. Protein & cell. 2015;6(6):434-42.
102. Foskett JK, Philipson B. The mitochondrial Ca(2+) uniporter complex. Journal of molecular and cellular cardiology. 2015;78:3-8.
103. Pan X, Liu J, Nguyen T, Liu C, Sun J, Teng Y, et al. The physiological role of mitochondrial calcium revealed by mice lacking the mitochondrial calcium uniporter. Nature cell biology. 2013;15(12):1464-72.
104. Kamer KJ, Mootha VK. MICU1 and MICU2 play nonredundant roles in the regulation of the mitochondrial calcium uniporter. EMBO reports. 2014;15(3):299-307.
105. Patron M, Checchetto V, Raffaello A, Teardo E, Vecellio Reane D, Mantoan M, et al. MICU1 and MICU2 finely tune the mitochondrial Ca2+ uniporter by exerting opposite effects on MCU activity. Molecular cell. 2014;53(5):726-37.
106. Vais H, Mallilankaraman K, Mak DO, Hoff H, Payne R, Tanis JE, et al. EMRE Is a Matrix Ca(2+) Sensor that Governs Gatekeeping of the Mitochondrial Ca(2+) Uniporter. Cell reports. 2016;14(3):403-10.
107. Paupe V, Prudent J, Dassa EP, Rendon OZ, Shoubridge EA. CCDC90A (MCUR1) is a cytochrome c oxidase assembly factor and not a regulator of the mitochondrial calcium uniporter. Cell metabolism. 2015;21(1):109-16.
108. Tomar D, Dong Z, Shanmughapriya S, Koch DA, Thomas T, Hoffman NE, et al. MCUR1 Is a Scaffold Factor for the MCU Complex Function and Promotes Mitochondrial Bioenergetics. Cell reports. 2016;15(8):1673-85.
109. Chaudhuri D, Artiga DJ, Abiria SA, Clapham DE. Mitochondrial calcium uniporter regulator 1 (MCUR1) regulates the calcium threshold for the mitochondrial permeability transition. Proceedings of the National Academy of Sciences of the United States of America. 2016;113(13):E1872-80.
110. Tsai MF, Jiang D, Zhao L, Clapham D, Miller C. Functional reconstitution of the mitochondrial Ca2+/H+ antiporter Letm1. The Journal of general physiology. 2014;143(1):67-73.
111. Doonan PJ, Chandramoorthy HC, Hoffman NE, Zhang X, Cardenas C, Shanmughapriya S, et al. LETM1-dependent mitochondrial Ca2+ flux modulates cellular bioenergetics and proliferation. FASEB journal : official publication of the Federation of American Societies for Experimental Biology. 2014;28(11):4936-49.
112. Lockwich T, Pant J, Makusky A, Jankowska-Stephens E, Kowalak JA, Markey SP, et al. Analysis of TRPC3-interacting proteins by tandem mass spectrometry. Journal of proteome research. 2008;7(3):979-89.
113. Jiang Y, Huang H, Liu P, Wei H, Zhao H, Feng Y, et al. Expression and localization of TRPC proteins in rat ventricular myocytes at various developmental stages. Cell and tissue research. 2014;355(1):201-12.

114. Beutner G, Sharma VK, Giovannucci DR, Yule DI, Sheu SS. Identification of a ryanodine receptor in rat heart mitochondria. The Journal of biological chemistry. 2001;276(24):21482-8.
115. Beutner G, Sharma VK, Lin L, Ryu SY, Dirksen RT, Sheu SS. Type 1 ryanodine receptor in cardiac mitochondria: transducer of excitation-metabolism coupling. Biochimica et biophysica acta. 2005;1717(1):1-10.
116. Altschafl BA, Beutner G, Sharma VK, Sheu SS, Valdivia HH. The mitochondrial ryanodine receptor in rat heart: a pharmaco-kinetic profile. Biochimica et biophysica acta. 2007;1768(7):1784-95.
117. Sparagna GC, Gunter KK, Sheu SS, Gunter TE. Mitochondrial calcium uptake from physiological-type pulses of calcium. A description of the rapid uptake mode. The Journal of biological chemistry. 1995;270(46):27510-5.
118. Buntinas L, Gunter KK, Sparagna GC, Gunter TE. The rapid mode of calcium uptake into heart mitochondria (RaM): comparison to RaM in liver mitochondria. Biochimica et biophysica acta. 2001;1504(2-3):248-61.
119. Michels G, Khan IF, Endres-Becker J, Rottlaender D, Herzig S, Ruhparwar A, et al. Regulation of the human cardiac mitochondrial Ca2+ uptake by 2 different voltage-gated Ca2+ channels. Circulation. 2009;119(18):2435-43.
120. Prabakaran S, Lippens G, Steen H, Gunawardena J. Post-translational modification: nature's escape from genetic imprisonment and the basis for dynamic information encoding. Wiley interdisciplinary reviews Systems biology and medicine. 2012;4(6):565-83.
121. Beltrao P, Bork P, Krogan NJ, van Noort V. Evolution and functional cross-talk of protein post-translational modifications. Molecular systems biology. 2013;9:714.
122. Acin-Perez R, Salazar E, Kamenetsky M, Buck J, Levin LR, Manfredi G. Cyclic AMP produced inside mitochondria regulates oxidative phosphorylation. Cell metabolism. 2009;9(3):265-76.
123. Hofer A, Wenz T. Post-translational modification of mitochondria as a novel mode of regulation. Experimental gerontology. 2014;56:202-20.
124. Hart GW, Slawson C, Ramirez-Correa G, Lagerlof O. Cross talk between O-GlcNAcylation and phosphorylation: roles in signaling, transcription, and chronic disease. Annual review of biochemistry. 2011;80:825-58.
125. Lewandrowski U, Sickmann A, Cesaro L, Brunati AM, Toninello A, Salvi M. Identification of new tyrosine phosphorylated proteins in rat brain mitochondria. FEBS letters. 2008;582(7):1104-10.
126. Zhang Z, Tan M, Xie Z, Dai L, Chen Y, Zhao Y. Identification of lysine succinylation as a new post-translational modification. Nature chemical biology. 2011;7(1):58-63.
127. Arena G, Gelmetti V, Torosantucci L, Vignone D, Lamorte G, De Rosa P, et al. PINK1 protects against cell death induced by mitochondrial depolarization, by phosphorylating Bcl-xL and impairing its pro-apoptotic cleavage. Cell death and differentiation. 2013;20(7):920-30.
128. Yang Y, Bedford MT. Protein arginine methyltransferases and cancer. Nature reviews Cancer. 2013;13(1):37-50.
129. Chen C, Nott TJ, Jin J, Pawson T. Deciphering arginine methylation: Tudor tells the tale. Nature reviews Molecular cell biology. 2011;12(10):629-42.
130. Herrmann F, Lee J, Bedford MT, Fackelmayer FO. Dynamics of human protein arginine methyltransferase 1(PRMT1) in vivo. The Journal of biological chemistry. 2005;280(45):38005-10.

131. Goulet I, Gauvin G, Boisvenue S, Cote J. Alternative splicing yields protein arginine methyltransferase 1 isoforms with distinct activity, substrate specificity, and subcellular localization. The Journal of biological chemistry. 2007;282(45):33009-21.
132. Sakamaki J, Daitoku H, Ueno K, Hagiwara A, Yamagata K, Fukamizu A. Arginine methylation of BCL-2 antagonist of cell death (BAD) counteracts its phosphorylation and inactivation by Akt. Proceedings of the National Academy of Sciences of the United States of America. 2011;108(15):6085-90.
133. Yoshimatsu M, Toyokawa G, Hayami S, Unoki M, Tsunoda T, Field HI, et al. Dysregulation of PRMT1 and PRMT6, Type I arginine methyltransferases, is involved in various types of human cancers. International journal of cancer. 2011;128(3):562-73.
134. Mathioudaki K, Papadokostopoulou A, Scorilas A, Xynopoulos D, Agnanti N, Talieri M. The PRMT1 gene expression pattern in colon cancer. British journal of cancer. 2008;99(12):2094-9.
135. Papadokostopoulou A, Mathioudaki K, Scorilas A, Xynopoulos D, Ardavanis A, Kouroumalis E, et al. Colon cancer and protein arginine methyltransferase 1 gene expression. Anticancer research. 2009;29(4):1361-6.
136. Mathioudaki K, Scorilas A, Ardavanis A, Lymberi P, Tsiambas E, Devetzi M, et al. Clinical evaluation of PRMT1 gene expression in breast cancer. Tumour biology : the journal of the International Society for Oncodevelopmental Biology and Medicine. 2011;32(3):575-82.
137. Avasarala S, Van Scoyk M, Karuppusamy Rathinam MK, Zerayesus S, Zhao X, Zhang W, et al. PRMT1 Is a Novel Regulator of Epithelial-Mesenchymal-Transition in Non-small Cell Lung Cancer. The Journal of biological chemistry. 2015;290(21):13479-89.
138. Deng X, Von Keudell G, Suzuki T, Dohmae N, Nakakido M, Piao L, et al. PRMT1 promotes mitosis of cancer cells through arginine methylation of INCENP. Oncotarget. 2015;6(34):35173-82.
139. Waldeck-Weiermair M, Duan X, Naghdi S, Khan MJ, Trenker M, Malli R, et al. Uncoupling protein 3 adjusts mitochondrial Ca(2+) uptake to high and low Ca(2+) signals. Cell calcium. 2010;48(5):288-301.
140. Jean-Quartier C, Bondarenko AI, Alam MR, Trenker M, Waldeck-Weiermair M, Malli R, et al. Studying mitochondrial Ca(2+) uptake - a revisit. Molecular and cellular endocrinology. 2012;353(1-2):114-27.
141. Deak AT, Blass S, Khan MJ, Groschner LN, Waldeck-Weiermair M, Hallstrom S, et al. IP3-mediated STIM1 oligomerization requires intact mitochondrial Ca2+ uptake. Journal of cell science. 2014;127(Pt 13):2944-55.
142. McCombs JE, Palmer AE. Measuring calcium dynamics in living cells with genetically encodable calcium indicators. Methods. 2008;46(3):152-9.
143. Contreras L, Drago I, Zampese E, Pozzan T. Mitochondria: the calcium connection. Biochimica et biophysica acta. 2010;1797(6-7):607-18.
144. Miyawaki A, Llopis J, Heim R, McCaffery JM, Adams JA, Ikura M, et al. Fluorescent indicators for Ca2+ based on green fluorescent proteins and calmodulin. Nature. 1997;388(6645):882-7.
145. Grynkiewicz G, Poenie M, Tsien RY. A new generation of Ca2+ indicators with greatly improved fluorescence properties. The Journal of biological chemistry. 1985;260(6):3440-50.

146. Deak AT, Groschner LN, Alam MR, Seles E, Bondarenko AI, Graier WF, et al. The endocannabinoid N-arachidonoyl glycine (NAGly) inhibits store-operated Ca2+ entry by preventing STIM1-Orai1 interaction. Journal of cell science. 2013;126(Pt 4):879-88.
147. Njoku DB. The immortal life of Henrietta Lacks. Anesthesia and analgesia. 2013;117(1):286.
148. Ahn K, Pan S, Beningo K, Hupe D. A permanent human cell line (EA.hy926) preserves the characteristics of endothelin converting enzyme from primary human umbilical vein endothelial cells. Life sciences. 1995;56(26):2331-41.
149. Esse R, Rocha MS, Barroso M, Florindo C, Teerlink T, Kok RM, et al. Protein arginine methylation is more prone to inhibition by S-adenosylhomocysteine than DNA methylation in vascular endothelial cells. PloS one. 2013;8(2):e55483.
150. Tehlivets O, Malanovic N, Visram M, Pavkov-Keller T, Keller W. S-adenosyl-L-homocysteine hydrolase and methylation disorders: yeast as a model system. Biochimica et biophysica acta. 2013;1832(1):204-15.
151. Bonham K, Hemmers S, Lim YH, Hill DM, Finn MG, Mowen KA. Effects of a novel arginine methyltransferase inhibitor on T-helper cell cytokine production. The FEBS journal. 2010;277(9):2096-108.
152. Mostaqul Huq MD, Gupta P, Tsai NP, White R, Parker MG, Wei LN. Suppression of receptor interacting protein 140 repressive activity by protein arginine methylation. The EMBO journal. 2006;25(21):5094-104.
153. Lee AV, Oesterreich S, Davidson NE. MCF-7 cells--changing the course of breast cancer research and care for 45 years. Journal of the National Cancer Institute. 2015;107(7).
154. Ayyasamy V, Owens KM, Desouki MM, Liang P, Bakin A, Thangaraj K, et al. Cellular model of Warburg effect identifies tumor promoting function of UCP2 in breast cancer and its suppression by genipin. PloS one. 2011;6(9):e24792.
155. Kuai XY, Ji ZY, Zhang HJ. Mitochondrial uncoupling protein 2 expression in colon cancer and its clinical significance. World journal of gastroenterology. 2010;16(45):5773-8.
156. Li W, Nichols K, Nathan CA, Zhao Y. Mitochondrial uncoupling protein 2 is up-regulated in human head and neck, skin, pancreatic, and prostate tumors. Cancer biomarkers : section A of Disease markers. 2013;13(5):377-83.
157. Langin D, Larrouy D, Barbe P, Millet L, Viguerie-Bascands N, Andreelli F, et al. Uncoupling protein-2 (UCP2) and uncoupling protein-3 (UCP3) expression in adipose tissue and skeletal muscle in humans. International journal of obesity and related metabolic disorders : journal of the International Association for the Study of Obesity. 1999;23 Suppl 6:S64-7.
158. Motloch LJ, Larbig R, Gebing T, Reda S, Schwaiger A, Leitner J, et al. By Regulating Mitochondrial Ca2+-Uptake UCP2 Modulates Intracellular Ca2+. PloS one. 2016;11(2):e0148359.
159. Fukumori R, Takarada T, Nakazato R, Fujikawa K, Kou M, Hinoi E, et al. Selective inhibition by ethanol of mitochondrial calcium influx mediated by uncoupling protein-2 in relation to N-methyl-D-aspartate cytotoxicity in cultured neurons. PloS one. 2013;8(7):e69718.
160. Kukat A, Dogan SA, Edgar D, Mourier A, Jacoby C, Maiti P, et al. Loss of UCP2 attenuates mitochondrial dysfunction without altering ROS production and uncoupling activity. PLoS genetics. 2014;10(6):e1004385.

161. Gao Y, Zhao Y, Zhang J, Lu Y, Liu X, Geng P, et al. The dual function of PRMT1 in modulating epithelial-mesenchymal transition and cellular senescence in breast cancer cells through regulation of ZEB1. Scientific reports. 2016;6:19874.
162. Hanahan D, Weinberg RA. The hallmarks of cancer. Cell. 2000;100(1):57-70.
163. Rossignol R, Gilkerson R, Aggeler R, Yamagata K, Remington SJ, Capaldi RA. Energy substrate modulates mitochondrial structure and oxidative capacity in cancer cells. Cancer research. 2004;64(3):985-93.
164. Kavanagh NI, Ainscow EK, Brand MD. Calcium regulation of oxidative phosphorylation in rat skeletal muscle mitochondria. Biochimica et biophysica acta. 2000;1457(1-2):57-70.

7 FIGURES

8 TABLES

9 PUBLICATIONS

The following studies have been achieved during the performance of my PhD thesis and have been published in international SCI-listed journals. *Current dissertation is based on results of publication No. 9.*

1. Kennedy BE, Madreiter CT, Vishnu N, Malli R, Graier WF, Karten B. **Adaptations of energy metabolism associated with increased levels of mitochondrial cholesterol in Niemann-Pick type C1-deficient cells.** *J Biol Chem.* 2014 Jun 6; 289(23):16278-89

2. Goeritzer M, Schlager S, Radovic B, Madreiter CT, Rainer S, Thomas G, Lord CC, Sacks J, Brown AL, Vujic N, Obrowsky S, Sachdev V, Kolb D, Chandak PG, Graier WF, Sattler W, Brown JM, Kratky D. **Deletion of CGI-58 or adipose triglyceride lipase differently affects macrophage function and atherosclerosis**. *J Lipid Res.* 2014 Dec; 55(12):2562-75

3. Bondarenko AI, Parichatikanond W, Madreiter CT, Rost R, Waldeck-Weiermair M, Malli R, Graier WF. **UCP2 modulates single-channel properties of a MCU-dependent Ca^{2+} inward current in mitochondria.** *Pflugers Arch.* 2015 Dec; 467(12):2509-18

4. Waldeck-Weiermair M, Malli R, Parichatikanond W, Gottschalk B, Madreiter-Sokolowski CT, Klec C, Rost R, Graier WF. **Rearrangement of MICU1 multimers for activation of MCU is solely controlled by cytosolic Ca^{2+}.** *Sci Rep.* 2015 Oct 22; 5:15602

5. Vujic N, Schlager S, Eichmann TO, Madreiter-Sokolowski CT, Goeritzer M, Rainer S, Schauer S, Rosenberger A, Woelfler A, Doddapattar P, Zimmermann R, Hoefler G, Lass A, Graier WF, Radovic B, Kratky D. **Monoglyceride lipase deficiency modulates endocannabinoid signaling and improves plaque stability in ApoE-knockout mice.** *Atherosclerosis.* 2016 Jan; 244:9-21

6. Eroglu E, Gottschalk B, Charoensin S, Blass S, Bischof H, Rost R, Madreiter-Sokolowski CT, Pelzmann B, Bernhart E, Sattler W, Hallström S, Malinski T, Waldeck-Weiermair M, Graier WF, Malli R. **Development of novel FP-based probes for live-cell imaging of nitric oxide dynamics.** *Nat Commun.* 2016 Feb 4;7:10623

7. Prokesch A, Pelzmann HJ, Pessentheiner AR, Huber K, Madreiter-Sokolowski CT, Drougard A, Schittmayer M, Kolb D, Magnes C, Trausinger G, Graier WF, Birner-Gruenberger R, Pospisilik JA, Bogner-Strauss JG. **N-acetylaspartate catabolism determines cytosolic acetyl-CoA levels and histone acetylation in brown adipocytes.** *Sci Rep.* 2016 Apr 5; 6:23723

8. Madreiter-Sokolowski CT, Gottschalk B, Parichatikanond W, Erogul E, Klec C, Waldeck-Weiermair M, Malli R, Graier WF. **Resveratrol specifically kills cancer cells by a devastating increase in the Ca^{2+} coupling between the greatly tethered endoplasmic reticulum and mitochondria.** *Cell Physiol Biochem.* 2016 in press

9. Madreiter-Sokolowski CT, Klec C, Parichatikanond W, Stryeck S, Gottschalk B, Pulido S, Rost R, Eroglu E, Hofmann N, Bondarenko A, Madl T, Waldeck-Weiermair M, Malli R, Graier WF. **PRMT1-mediated methylation of MICU1 determines the UCP2/3-dependency of mitochondrial Ca^{2+} uptake in immortalized cells.** *Nat Commun.* 2016 in press